Marine Geology 449 (2022) 106835

Contents lists available at ScienceDirect

Marine Geology

journal homepage: www.elsevier.com/locate/margo

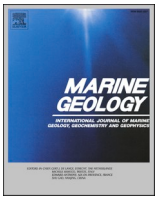

Contourite systems around the northern exit from the Vema Channel

Elena V. Ivanova [a,*], Dmitrii G. Borisov [a], Ivar O. Murdmaa [a], Ekaterina A. Ovsepyan [a], Dorrik Stow [b]

[a] Shirshov Institute of Oceanology, Russian Academy of Sciences, Moscow, Russia
[b] Institute of Geo-Energy Engineering, Heriot-Watt University, Edinburgh, UK

ARTICLE INFO

Keywords:
Ioffe Drift
Santa Catarina Plateau
São Paulo Plateau
LCDW and AABW
Sedimentation
Hiatuses
Bottom currents
Abyssal channel
Gateway

ABSTRACT

Several drifts of different types and sizes are identified near the northern exit of the Vema Channel, within the projects *Neogene-Quaternary contourites of the Central and South Atlantic* and *Lateral sedimentation in the deep ocean (on the examples from the Central and South-Western Atlantic)*. Herein, we discuss new results of a multidisciplinary study of sixteen sediment cores and high-resolution sub-bottom (seismoacoustic) profiles, to address the impact of Lower Circumpolar Deep Water (LCDW) and Antarctic Bottom Water (AABW) passing through the Vema gateway on contourite accumulation and erosion. To the west of the northern exit from the Vema Channel, an anticyclonic gyre of LCDW is instrumental in the development of contourite drifts and sediment waves. The contourite origin of generally silty terrigenous sediments in the Santa Catarina Plateau – São Paulo Plateau area is ascertained by both morpho-seismic and sedimentary characteristics. Sedimentary features include: a lack of primary sedimentary structures and pervasive bioturbation; sharp erosional contacts, local hiatuses and stiff mud horizons; some sandy/silty layers and indistinct bedding; mostly fine grain-size, very poor sorting and distinctive bi-gradational sequences; a high degree of correlation between the content of sortable silt (*SS)* in the total < 63 μm size fraction and *SS* mean sizes in all eight cores studied. Biostratigraphy, oxygen isotope records and ten new accelerator mass-spectrometry (AMS) ^{14}C dates reveal the mid to late Quaternary age of this mainly terrigenous contourite depositional system (CDS).

By contrast, the dominantly calcareous Ioffe Drift, overlying the Florianopolis Fracture Zone (FFZ) ridge to the northeast of the Vema Channel, is far from any source of terrigenous material, and accumulated in an area of low biological productivity. The overall asymmetric geometry, mainly lenticular, upward-convex seismic units separated by erosional unconformities, reflection truncation, small-scale moats dissecting the drift surface collectively indicate its contourite origin. The interpretation of the drift as the CDS is supported by sediment characteristics including common hiatuses corresponding in some cases to erosional contacts, pervasive bioturbation, generally poor sediment sorting, and more or less well-developed bi-gradational sequences. The erosion and deposition in the drift area are mostly controlled by the main LCDW branch following northeastward along the FFZ. Extensive erosion by bottom currents has created numerous hiatuses and markedly reduced the thickness of drift's sediments. The stratigraphic record from the Ioffe Drift sediment cores reveals an Upper Pliocene – Quaternary succession. The results of detailed analyses of six cores from the Ioffe Drift area, compared with two cores and the upper part of DSDP Site 516 from the Rio Grande Rise, notably the use of a *SS* analogue, provide new information on calcareous biogenic contourites deposited in the pelagic realm of the South Atlantic.

1. Introduction

The formation of deep-water contourite systems is known to be controlled by bottom currents, generally associated with global meridional overturning circulation (e.g. Heezen et al., 1966; Rebesco et al., 2014 and references therein). The relative speed and energy of bottom currents vary significantly and lead to commonly co-occurring depositional and erosive features, forming the contourite depositional systems (CDSs) of different scales (Hernández-Molina et al., 2003, 2008, 2009; Rebesco and Camerlenghi, 2008; Preu et al., 2013). Along with CDS' value as paleoceanographic archives (e.g. Faugères and Stow, 2008) and potential reservoirs for hydrocarbons (e.g. Llave et al., 2019), they

* Corresponding author.
E-mail addresses: e_v_ivanova@ocean.ru (E.V. Ivanova), dborisov@ocean.ru (D.G. Borisov), eovsepyan@ocean.ru (E.A. Ovsepyan), d.stow@hw.ac.uk (D. Stow).

https://doi.org/10.1016/j.margeo.2022.106835
Received 9 March 2021; Received in revised form 5 May 2022; Accepted 17 May 2022
Available online 24 May 2022

garnered much attention as potential sources of geohazards like landslides and slope failures (Laberg and Camerlenghi, 2008; Krastel et al., 2011). The available works on regional-scale CDSs and their importance in terms of paleocirculation reconstructions were summarized by Rebesco et al. (2014). Regional studies of particular CDSs were performed on the Argentine slope (Hernández-Molina et al., 2009, 2016; Wilckens et al., 2021), offshore NW Spain (Hanebuth et al., 2015), in the Sicily Channel (Gauchery et al., 2021a), in the Adriatic Sea (Pellegrini et al., 2016), on several plateaus, including e.g. the Demerara Plateau (Tallobre et al., 2016), Rockall Plateau (Sayago-Gil et al., 2010) and Motril Marginal Plateau (Palomino et al., 2011).

Within the area between the Argentine Basin and Brazil Basin (between 48°W and 32°W, 33°S and 27°S) dissected by the Vema Channel, several contourite features have been reported by earlier studies (Rebesco et al., 2014; Flanders Marine Institute, 2019), notably the Santa Catarina Drift and Pelotas Drift (Jeck et al., 2019), Vema contourite fan (Mézerais et al., 1993; Faugères et al., 2002), Ioffe Drift (Ivanova et al., 2016a, 2020), and plastered drifts on the São Paulo Plateau escarpment (Borisov et al., 2013; Ovsepyan and Ivanova, 2019). Furthermore, large fields of sediment waves are present on the Santa

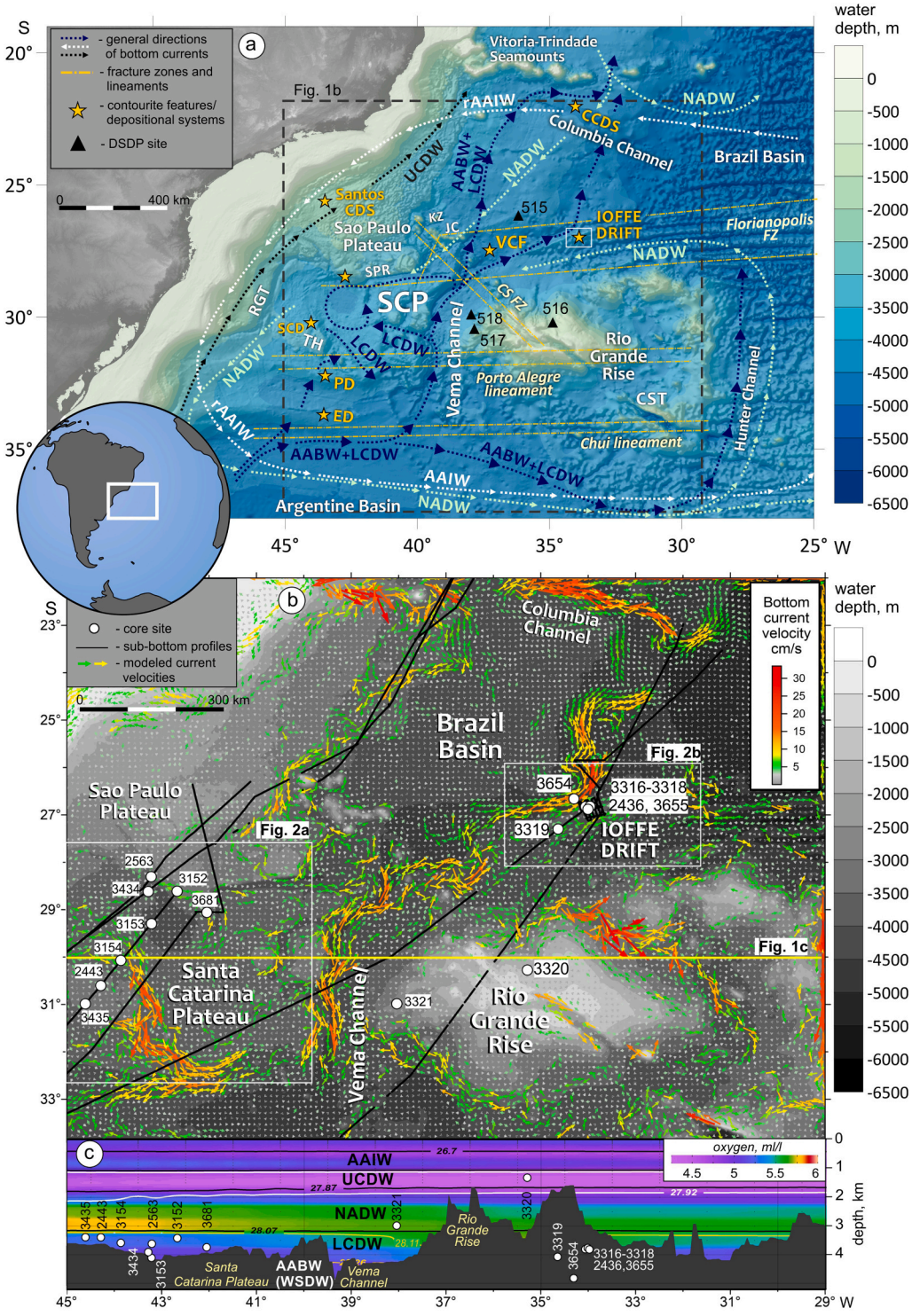

Fig. 1. Bathymetry and general directions of major currents of the Northern Argentine and Southern Brazil Basin with location of the main contourite features, sediment cores and DSDP sites. a) Regional bathymetric map with directions of surface-to-bottom water currents (shown by arrow). Morphological features: SCP – Santa Catarina Plateau, SPR – São Paulo Ridge, TH – Torres High, RGT – Rio Grande Terrace, CST – Cruzeiro do Sul Trough, Jean Charcot seamounts, KZ – Kazanskiy seamount; fracture zones (FZ): Florianopolis FZ and Cruzeiro do Sul FZ. Contourite drift systems (CS and CDS): CCDS – Columbia contourite drift system, Santos CDS – Santos contourite drift system, SCD – Santa Catarina Drift, VCF –Vema contourite fan, PD –Pelotas Drift, ED – Ewing Drift. Water masses: TW – Tropical Water, SACW—South Atlantic Central Water, AAIW - Antarctic Intermediate Water, rAAIW – recirculated branch of the AAIW, UCDW – Upper Circumpolar Deep Water, NADW – North Atlantic Deep Water; LCPW — Lower Circumpolar Water, AABW – Antarctic Bottom Water. Inset shows location of the study area in the SW Atlantic. b) Modern bottom current directions and velocities indicated by arrows according to Morozov et al. (2010, 2019, 2020) and modeling results (Frey et al., 2018) with location of the sediment cores studied (white dots) on the seismoacoustic profiles (black lines); c) distribution of oxygen content in the water column (Levitus et al., 2010) along the profile shown by a yellow line in Fig. 1b, with boundaries of water masses corresponding to isolines of neutral density according to Hernández-Molina et al. (2016) and Jullion et al. (2010) shown in black and white, respectively. WSDW – Weddell Sea Deep Water. (For interpretation of the references to colour in this figure legend, the reader is referred to the web version of this article.)

Catarina Plateau (Jeck et al., 2019; Borisov et al., 2020) and the Rio Grande Rise (Lisniowski et al., 2017; Levchenko et al., 2020). Several of these drift systems comprise calcareous contourites. Whereas, terrigenous contourites are rather well documented in the Atlantic (e.g. Hernández-Molina et al., 2010; Rebesco et al., 2014; Jeck et al., 2019), much less is known about calcareous contourites, in particular those at water depths over 3 km (Eberli and Betzler, 2019).

In the SW Atlantic, the Rio Grande Rise, São Paulo Plateau and Santa Catarina Plateau separate the Argentine Basin from the Brazil Basin and limit the northward propagation of deep and bottom waters of southern origin (Fig. 1a). The narrow Vema Channel cuts through this topographic barrier and represents the main oceanic gateway between these basins. It allows the northward passage of cold, dense Antarctic Bottom Water (AABW) and Lower Circumpolar Deep Water (LCDW) beneath southward-flowing North Atlantic Deep Water (NADW). The onset of AABW formation is believed to have occurred around the Eocene – Oligocene boundary after the opening of the Drake Passage at 30–35 Ma (Kennett and Barker, 1990; Livermore et al., 2005, 2007; Allen and Armstrong, 2008; Ivanova, 2009; Najjarifarizhendi and Uenzelmann-Neben, 2021), and continues up to present with variable intensity.

The variability of bottom current speed through the Vema Channel was studied by Ledbetter (1979, 1984), and found to have a complex link to paleoclimate. Recently, modeling results have demonstrated the importance of periodic events of enhanced bottom-current velocities in sediment erosion, reworking, transport and subsequent accumulation (Thran et al., 2018; Wilckens et al., 2021; Frey et al., 2022). According to Thran et al. (2018), local fluctuations are believed to exert more significant control on contourite formation than an overall increase/decrease in current flow.

This paper documents the influence of the Vema Channel on the contourite formation from the Late Pliocene to Recent, focusing on contourite depositional systems investigated under the framework of the projects *"Neogene-Quaternary contourites of the Central and South Atlantic"* and *Lateral sedimentation in the deep ocean (on the examples from the Central and South-western Atlantic)*. These CDSs have been partially reported in our earlier publications, but we present completely new data and new analysis in this paper. They include a mostly terrigenous CDS in the Santa Catarina Plateau – São Paulo Plateau area (Borisov et al., 2013, 2020; Ovsepyan and Ivanova, 2019) and two calcareous CDSs in the Ioffe Drift – Rio Grande Rise area (Ivanova et al., 2016a, 2020; Levchenko et al., 2020; Murdmaa and Ivanova, 2021), lying to the west and east of the Vema Channel, respectively. The recently published results on the sediment waves investigation in the Santa Catarina Plateau region (Borisov et al., 2020) and Rio Grande Rise (Levchenko et al., 2020) obtained within the first of our two projects are now supplemented by the new sub-bottom profiles and sediment cores presented in this study. In the Ioffe Drift and Rio Grande Rise, the stratigraphic framework and distribution of erosional hiatuses reported from six drift's sediment cores (Ivanova et al., 2016a, 2020, 2021; Ivanova and Dmitrenko, 2021) are supplemented by grain-size analyses and multi-sensor core-logging not only for the former (Murdmaa et al., 2021a) but also for the latter area.

We applied the sortable silt (*SS*) approach by McCave et al. (2017) as one of the most valuable proxies developed for the terrigenous contourites study. To investigate the calcareous contourites and compare them to terrigenous ones, we attempted to consider fine carbonate material as a kind of analogue of the fine clastic material and to apply the sortable silt (*SS*) proxy to calcareous sediments as well.

2. Regional setting

2.1. Physiography

The study area extends 1250 km in a W-E direction and more than 890 km in an N-S direction (Fig. 1a). To the west, it is limited by the South American continental slope. The 600 km long and 20–30 km wide Vema Channel occupying the deepest part of the Rio Grande Gap (water depth over 4800 m) separates the Rio Grande Rise in the east from the Santa Catarina and São Paulo plateaus in the west (Le Pichon et al., 1971; Johnson, 1984).

The São Paulo Plateau is located on the South American continental slope at a depth of 1200–3200 m, according to Viana et al. (2003) and Jeck et al. (2019). The submarine valley in the south-western part of the plateau is connected upslope with the Cananéia canyon (Duarte and Viana, 2007). The plateau is bounded by a 500–1500 m high southern escarpment and a deep valley related to the Florianopolis Fracture Zone. The valley separates the São Paulo Plateau from the Santa Catarina Plateau to the south. The major part of the latter is dominated by the Santa Catarina Drift and covered by sediment waves (Jeck et al., 2019). We refer to this region, collectively, as the Santa Catarina CDS.

The Ioffe Drift, which is included in the Global contourite distribution database (Flanders Marine Institute et al., 2019), overlies the central part of the narrow tectonic ridge within the Florianopolis (Rio Grande) Fracture Zone (FFZ, Meisling et al., 2001) in the southern Brazil Basin. The ridge with steep northern slopes and gentler southern slopes is oriented in a SW–NE direction and rises to more than 700 m above the adjacent seafloor. The length of its crest is approximately 470 to 500 km, and the summit is at a water depth of 3800 m. The deep narrow fault-controlled channel at the base of its northern slope is up to 300 m deep and is connected to the Vema Channel (Fig. 1a, Morozov et al., 2020). We refer to this region as the Ioffe CDS.

2.2. Oceanography

The deep and bottom-water circulation in the study area is controlled by five major water masses, notably the Antarctic Intermediate Water (AAIW, with a potential temperature (θ) of about 3–6 °C and salinity (S, practical salinity units, psu) 33.90–34.3) and its return southward branch (the so-called re-circulated AAIW or rAAIW), Upper Circumpolar Deep Water (UCDW, $\theta = 2.8–3$ °C and $34.4 < S < 34.7$), NADW ($\theta = 2.3–3.5$ °C and $34.6 < S < 35$ psu), LCDW ($\theta = 0–2$ °C and $34.7 < S < 34.8$ psu) and AABW (or Weddell Sea Deep Water, WSDW, $\theta < 0$ °C and $S < 34.7$ psu) according to Schlitzer (2010) and by the interactions between these water masses and with the seafloor topography (Fig. 1a). The boundaries between water masses are defined by neutral density (Fig. 1c; Jackett and McDougall, 1997) according to Orsi et al. (1999), Morozov et al. (2010), Jullion et al. (2010) and Hernández-Molina et al. (2016). AAIW (and UCDW sweep the summit of the Rio Grande Rise at water depths ranging from 500 to 1200 m and from 1200 m to 1600–1900 m, respectively (Levitus et al., 2010). The AAIW/UCDW interface corresponds to the isolines of neutral density $\gamma^n = 27.5–27.55$ g/cm^3 (Jullion et al., 2010; Hernández-Molina et al., 2016).

The boundaries between UCDW, NADW and LCDW in the western part of the study area occur at depths of 1760–1950 m and 3200–3400 m, respectively (Fig. 1c) and can be correlated with lines of neutral density $\gamma^n = 27.87–27.92$ and 28.07–28.11 g/cm^3 (Jullion et al., 2010; Hernández-Molina et al., 2016). Eastward of the Vema Channel, the boundary between UCDW and NADW lies at about the same depth, whereas the boundary between NADW and LCDW is somewhat deeper, at 3420–3520 m according to the conductivity-temperature-depth (CTD)-data from Morozov et al. (2010). Therefore, the summits of Ioffe Drift and Rio Grande Rise are bathed by LCDW and AAIW/UCDW, respectively. The major part of the Santa Catarina Plateau is also washed by LCDW down to 4000 m. LCDW generally flows northward along the continental margin and through the Vema Channel, penetrating respectively to the Santa Catarina Plateau and Ioffe Drift area. However, LCDW veers both northeastward along the FFZ and also westward from the northern exit of the Vema Channel, flowing to the Santa Catarina Plateau along the southern escarpment of the São Paulo Plateau (Fig. 1a; Morozov et al., 2010).

Available estimates of geostrophic bottom water flow over the Santa Catarina Plateau suggest that comparable transport of 1.3–1.8 Sv can occur both in the northward and southward directions (McDonagh et al.,

2002; Morozov et al., 2010). In the Ioffe Drift area, modeling results suggest a clockwise LCDW gyre (Fig. 1b; Frey et al., 2017; Fig. 1c in Ivanova et al., 2020).

The Vema Channel and the deep fault-controlled channel north of the Ioffe Drift below about 4000–4100 m convey AABW with a neutral density of $\gamma^n = 28.26–28.27$ g/cm^3 at the upper boundary (Orsi et al., 1999; Morozov et al., 2010).

The bottom current velocities measured by the Lowered Acoustic Doppler Current Profiler (LADCP) demonstrate that the near-bottom flow speed can reach 30 cm/s on the Santa Catarina Plateau (Frey et al., 2018) and ≥ 20 cm/s at a water depth of 4600–4750 m in the fault-controlled valley north of the Ioffe Drift (Morozov et al., 2020). There is also marked variability in current speed and direction in the Vema Channel, from 25 to 40 cm/s according to Le Pichon et al. (1971), and up to 55 cm/s according to Morozov et al. (2019). The bottom currents flowing through the channel transport a large amount of suspended matter comprising mostly biogenic detritus (including fragments of foraminiferal tests, diatoms, and coccoliths) as well as terrigenous mineral particles (Morozov et al., 2010).

The study area is characterized by relatively low biological productivity, which is typical of the oligotrophic subtropical zone bounded to the west by the Brazil western boundary current. Pelagic sediments are mainly composed of foraminiferal tests and coccoliths. Terrigenous supply is also rather low especially eastward of the Vema Channel, far from the continent. In the west, 129*10^6 t of suspended matter is provided annually by the Río de la Plata (Depetris and Griffin, 1968). Part of this material is transported across-shelf and downslope, contributing to terrigenous sedimentation on the Santa Catarina and São Paulo plateaus (Krastel et al., 2011; Razik et al., 2013; Perez et al., 2016). Sediment supplied from the Rio Doce is also known to reach the Rio Grande Rise (Gingele et al., 1999).

On the Santa Catarina Plateau and in the Ioffe Drift area, the calcite saturation level occurs at about 3750 and 4000 m, respectively, according to hydrochemical data (Chung et al., 2003). In the region of the Rio Grande Rise and Vema Channel, the foraminiferal lysocline and calcite compensation depth (CCD) occur at water depths of approximately 4050 and 4500 m, respectively, according to Melguen and Thiede (1974). Hence, at present the study area (Fig. 1; Table 1) mostly lies above the foraminiferal lysocline.

3. Material and methods

High resolution sub-bottom profiling data were collected during six cruises of the RV *Akademik Ioffe* between 2010 and 2017 (Figs. 1b, 2a,b; Levchenko and Murdmaa, 2013a, 2013b; Levchenko et al., 2014; Ivanova et al., 2016b, 2018a, 2018b) using an *SES 2000 deep* narrow-beam parametric echo-sounder with a frequency of 4–5 kHz and vertical resolution of ~40 cm. The *SES 2000 deep* data were processed (heave correction and median filter application) with Interactive Sediment Layer Editor (ISE) software roughly assuming a sound velocity of 1500 m/s for both the water column and sediments (although the velocity might be different at greater water depth and vary according to sediment changes).

The types of seismic facies (also referred to as echo-characters or acoustic facies) were determined according to Damuth and Hayes (1977), and Maestro et al. (2021).

In the study area, a series of gravity cores (6 and 8 m-long with an inner/outer diameter of 110/127 mm) were collected during the same and other cruises of the RV *Akademik Ioffe* (Ivanova et al., 2016b, 2018 a,b; Skolotnev et al., 2018). The core sites were selected on the aforementioned seismoacoustic profiles to investigate the supposed contourite features (Figs. 1b, 2a,b). In addition, a series of grab samples were collected across the deep fault-controlled channel north of the Ioffe Drift. The sediment sections were opened, visually described and continuously sampled aboard the ship. For this study, we have examined 16 cores for sedimentological, geochemical and stratigraphic study (Table 1).

Further details of the methods used for sample processing, stratigraphic study, magnetic susceptibility (MS) and X-Ray Fluorescence (XRF) analyses are provided in our previous papers (Ivanova et al., 2016a, 2020; Ovsepyan and Ivanova, 2019). New results on 8 cores from the Ioffe Drift and the Rio Grande Rise were obtained by linear photo scanning, MS and XRF analyses using the Geotek MSCL-XYZ core workstation (Murdmaa et al., 2021a). The results of biostratigraphic

Table 1
Sediment cores location and length.

Core/ Grab	Latitude	Longitude	Depth, m	Length, m	Location	Reference
Southern São Paulo Plateau escarpment area						
AI-3152	28°37.34′ S	42°40.45′ W	3435	4.28	Drift on a small terrace on the escarpment	Ovsepyan and Ivanova, 2019; this study
AI-2563	28°24′ S	43°17′ W	3620	4.85	Top of the mounded body close to the foot of the escarpment	Borisov et al., 2013; this study
Santa Catarina Plateau						
AI-3434	28°851.85′ S	43°32.17’ W	3924	3.1	Northern part of the sediment wave field	This study
AI-3153	29°17.95′S	43°43.32’	4040	3.28	Buried part of the sediment wave field	This study
AI-3154	30°04.74′S	43°51.46′W	3592	4.75	Top of the sediment wave on the Torres High slope	This study
AI-2443	30°36.20′S	44°16.97′W	3410	3.42	Top of the Torres High	This study
AI-3435	30°59.42′S	44°36.98′W	3401	4.18	Top of the giant sediment wave	This study
AI-3681	29°03.041′ S	42°02.67′ W	3751	4.5	Mounded depositional body near the S-N oriented channel	This study
Ioffe Drift						
AI-2436	26°51.60′S	34°01.40′W	3799	7.14*	Drift summit	Ivanova et al., 2016a, corrected; this study
AI-3655	26°51.59′S	34°01.40′W	3799	5.14	Drift summit	This study
AI-3316	26°49.33′S	33°57.46′W	3898	4.89	Northern slope	Ivanova et al., 2020; this study
AI-3317	26°50.79′S	34°02.33′W	3832	5.15	Northern slope	This study
AI-3318	26°50.98′S	34°00.41′W	3788	3.46	Drift summit	Ivanova et al., 2020; this study
AI-3319	27°17.79′S	34°37.08′W	4066	2.87	Series of wave-like depositional features to WSW from the Ioffe Drift	This study
AI-3654	26°40.18′S	34°16.61′W	4695	0.2	Northern sope of fault channel to the north of Ioffe Drift	This study
Río Grande Rise						
AI-3320	30°16.50′S	35°17.12′W	1323	1.16	Summit of the rise (at DSDP Site 516)	This study
AI-3321	30°59.11’S	38°02.45′W	2969	2.93	Western flank of the rise (at DSDP Site 517)	This study

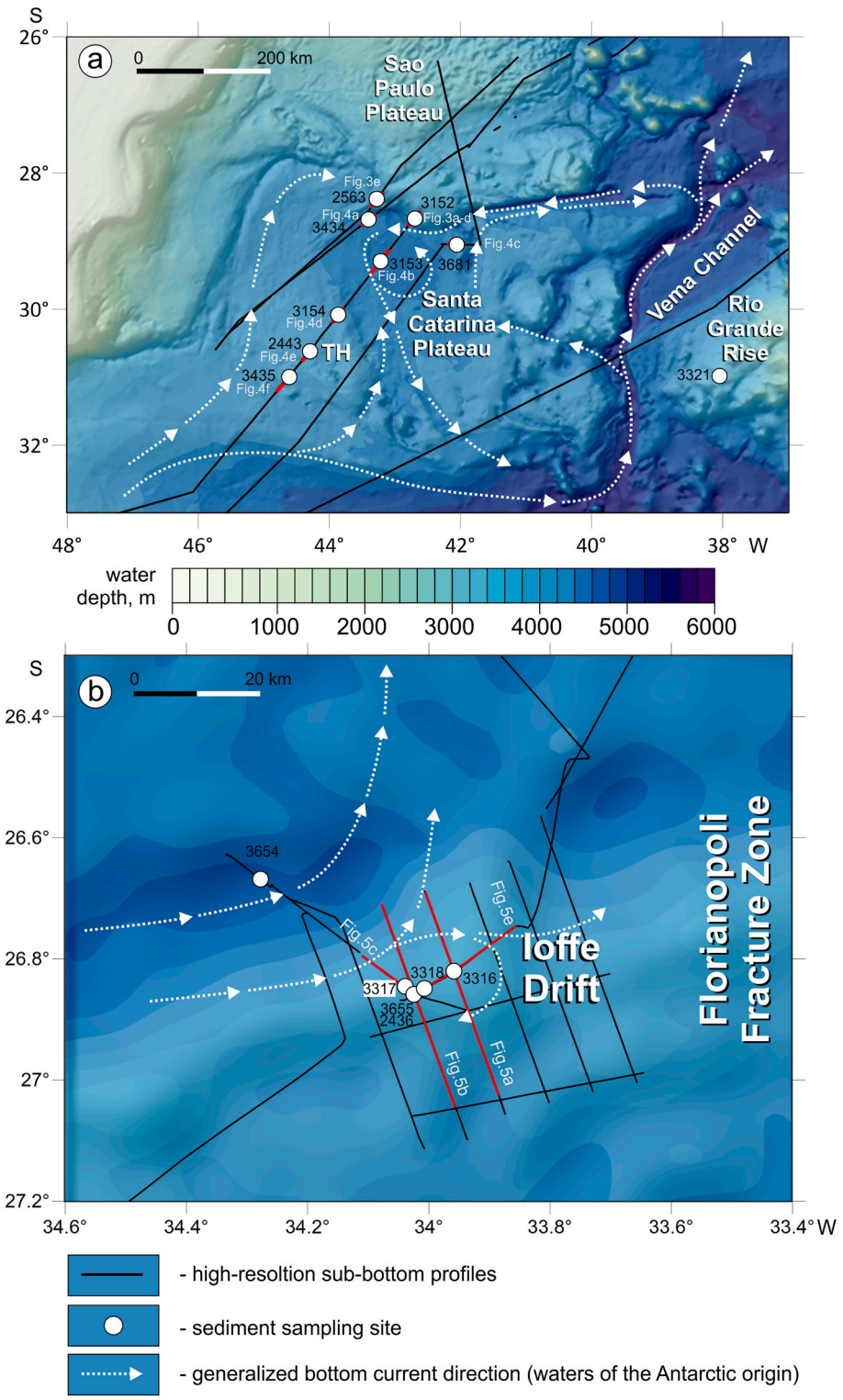

Fig. 2. Bathymetry, general directions of major bottom currents, seismoacoustic profiles and location of sampling sites. a) Santa Catarina – São Paulo Plateau area, b) Ioffe Drift area. For location of (a) and (b) see Fig. 1 The red lines highlight the location of profiles shown in Figs. 3-5. (For interpretation of the references to colour in this figure legend, the reader is referred to the web version of this article.)

study of six sediment cores from the Ioffe Drift are available (Ivanova and Dmitrenko, 2021).

The MS signal is taken to reflect the terrigenous supply to the study area (Thompson and Oldfield, 1986; Schmieder, 2004). From the XRF data, the normalized Ca/Al ratio calculated as ln(Ca/Al) according to (Weltje and Tjallingii, 2008; Rothwell and Croudace, 2015) is used as a regional stratigraphic constraint. It qualitatively reflects the $CaCO_3$ content of the sediments relative to the terrigenous fraction (Jaccard et al., 2005; Rothwell and Croudace, 2015) and allows the robust correlation of the sediment cores. In the Atlantic and in particular on the southwestern flank of the Rio Grande Rise, the latter is shown to have been higher during interglacial periods and interstadial episodes, due to

higher production and better preservation of calcareous microfossils along with lower terrigenous supply, than in glacial and stadial periods (Bacon, 1984; Jones et al., 1984; Hodell et al., 2001; Rickaby et al., 2010; Eberli and Betzler, 2019). In addition, ln(Zr/Rb) is used to illustrate relative changes in mean grain size related to bottom currents intensity according to (Rothwell and Croudace, 2015) nearby the erosional contacts in the sediment core AI-3154.

Grain-size analyses were performed using a SALD-2300 laser diffraction particle size analyzer (Shimadzu, Japan), which yields a size spectrum from 17 μm to 2.5 mm. In all cores, the sample spacing was even, ranging 10–15 cm and 10–40 cm in homogenous intervals from the Santa Catarina/Rio Grande cores and Ioffe Drift cores, respectively. The spacing was 1–8 cm where specific lithological changes were taken into account. From the Santa Catarina cores, grain-size analysis was carried out on each sample separately for bulk sediment and the carbonate-free fraction. In the Ioffe Drift and the Río Grande Rise area, grain-size analysis was performed only on the bulk sediment, due to a common dominance of calcareous biogenic particles in the sediment cores. The samples were treated with H_2O_2 to remove organic matter before bulk sediment analysis, while for carbonate-free analyses, HCl was then used to remove biogenic carbonate, prior to a second analysis. The biogenic opal content is low (<1.3%) in the study area and thus no additional procedure was used for its removal from the sediment. For particle disaggregation, all samples were processed by sodium tripolyphosphate in an ultrasonic bath before the analysis.

From grain size analyses of all samples studied, the content of sortable silt (SS) in the 10–63 μm size fraction (McCave et al., 1995) and *SS* mean sizes, as well as their correlation coefficients, were calculated to allow inference about the probable current speed. Although the *SS* proxy is essentially a grain size measure of the carbonate-free terrigenous fraction of mainly siliciclastic contourites (McCave et al., 2017), we have attempted the same method for calcareous contourites, but without removal of the carbonate fraction. The latter is useless since the terrigenous admixture is low. Mean sizes of SS were computed using the GRADISTAT software (Folk and Ward, 1957; Blott and Pye, 2001).

In core AI-3321, the oxygen isotope ratio (δ ^{18}O) was measured down-core on the epibenthic foraminifer *C. wuellerstorfi* (Cw) at the Godwin Laboratory for Palaeoclimate Research (Cambridge, UK). The species was selected according to a common practice to avoid any bias of isotope signal by the pore water influence (e.g. Curry and Oppo, 2005). Similarly, δ ^{18}O Cw was measured in core AI-3152 (Ovsepyan and Ivanova, 2019). All results are provided relative to the Vienna Pee Dee Belemnite (VPDB) standard.

In 8 sediment cores collected from the different drifts, well-preserved mixed planktic foraminiferal tests were picked from the grain-size fraction >150 μm, where available, and used for accelerator mass spectrometry (AMS ^{14}C) dating performed in the Poznan Radiocarbon Laboratory (Poland). It should be noted, that terrigenous sediments of several cores were mostly foraminiferal-barren and, therefore, could not be dated by this method. The dating results for cores AI-3152 and AI-3318 were published earlier in Ovsepyan and Ivanova (2019) and Ivanova et al. (2020), respectively. All radiocarbon dates, including those for cores AI-3152 and AI-3318 were calibrated in CALIB 8.2 (Stuiver et al., 2021) applying the MARINE20 calibration curve (Heaton et al., 2020) with a standard reservoir correction of – 550 years.

4. Nomenclature

In this study, the commonly accepted nomenclature and interpretations of contourite features are used. In particular, the terms "contourite" and "contourite drift" are applied for sediments "deposited or substantially reworked by the persistent action of bottom currents" and for extensive accumulations of contourite sediments, respectively (Faugères et al., 1999; Faugères and Stow, 2008; Rebesco et al., 2014).

Moats are linear features parallel to the slope formed by reduced or no deposition with minor erosion (Hernández-Molina et al., 2008; Rebesco et al., 2014; Eberli and Betzler, 2019).

Terrigenous contourites are composed of siliciclastic material, clay minerals and organic matter derived from land. Deep-sea calcareous biogenic contourites are considered to be originated from vertical settling and further lateral transport of biogenic material (mostly foraminiferal tests and nannofossils).

Sediment waves are defined as large-scale, sinusoidal, depositional bedforms (generally up to a few kilometers wavelength and up to tens of meters in height) which are generated under the influence of bottom currents (e.g. Wynn and Stow, 2002).

The term "turbidites" describes gravity-driven deposits, accumulated by geologically instantaneous suspension flows. They are commonly represented by decimeter-scale cyclites, characterized by graded bedding from coarser below to fine-grained above (Bouma, 1964). The cyclites alternate in sediment sections with slowly accumulating hemipelagites.

The reflector is considered to be the boundary between layers of contrasting acoustic impedance, which is the product of sediment/rock density and seismic wave velocity. A reflector is expressed as a reflection in seismic records (Schlumberger, 2022), but the two terms are widely used as synonyms. However, the term "reflector" is more commonly used to describe sub-bottom profiling data (e.g. Damuth and Hayes, 1977; Loncke et al., 2009). Since this work is based on sub-bottom profiling data the term "reflector" is preferred.

The seismic unit represents a mappable, three-dimensional unit composed of groups of reflections whose parameters differ from those of neighboring seismic units (Mitchum et al., 1977).

5. Results

5.1. Morpho-seismic characteristics

The Santa Catarina CDS comprises the Santa Catarina Plateau (SCP), a slightly elevated region lying to the west of the Vema Channel, and the southern flank of the São Paulo Plateau. The Santa Catarina Plateau has an irregular surface topography surrounded by channels through which the AABW and LCDW flow and circulate in a large gyre (Figs. 1, 2). There is a steep scarp to the north of the SCP that forms the southern flank of the São Paulo Plateau. This is mainly acoustically transparent to chaotic, but with two small perched plastered patch drifts, having prominent sub-parallel reflectors (Borisov et al., 2013; Ovsepyan and Ivanova, 2019) (Fig. 3a-d).

The drifts were traced at depths between 3450 and 3700 m. The shallower drift is characterized by a slightly mounded geometry and well-defined acoustic stratification (Fig. 3a,b). It has a thickness of up to 35 m and a width of 4 km along the profile. The body is separated from the plateau escarpment by a moat with a relative depth of approximately 8 m. The acoustic structure of the depositional feature can be divided into two units by an unconformity (Fig. 3b). The upper unit is up to 21 m thick and shows continuous subparallel reflectors with moderate amplitude. The configuration of reflections within this unit generally determines the mounded morphology of the sediment body (Fig. 3a,b). The lower unit is recorded in seismic profiles as an upward convex lens with discontinuous low-amplitude subparallel reflectors (Fig. 3b). The reflection configuration within the lower unit does not demonstrate clear evidence of the moat occurrence. Due to insufficient acoustic penetration, the lower boundary of the unit was not determined (Fig. 3a).

The deeper perched plastered patch drift has a form of an acoustically stratified lens overlying reflection free deposits and extending for 3.6 km along the profile (Fig. 3c,d). The thickness of the body reaches its maximum (22 m) in the axial part and rapidly decreases the upslope where a small local depression occurs (Fig. 3c,d). Subparallel mostly discontinuous reflectors tend to wedge out toward the lateral parts of the depositional feature. The uppermost reflector demonstrates toplapping in the area of the rapid decrease in the body thickness (Fig. 3c,d).

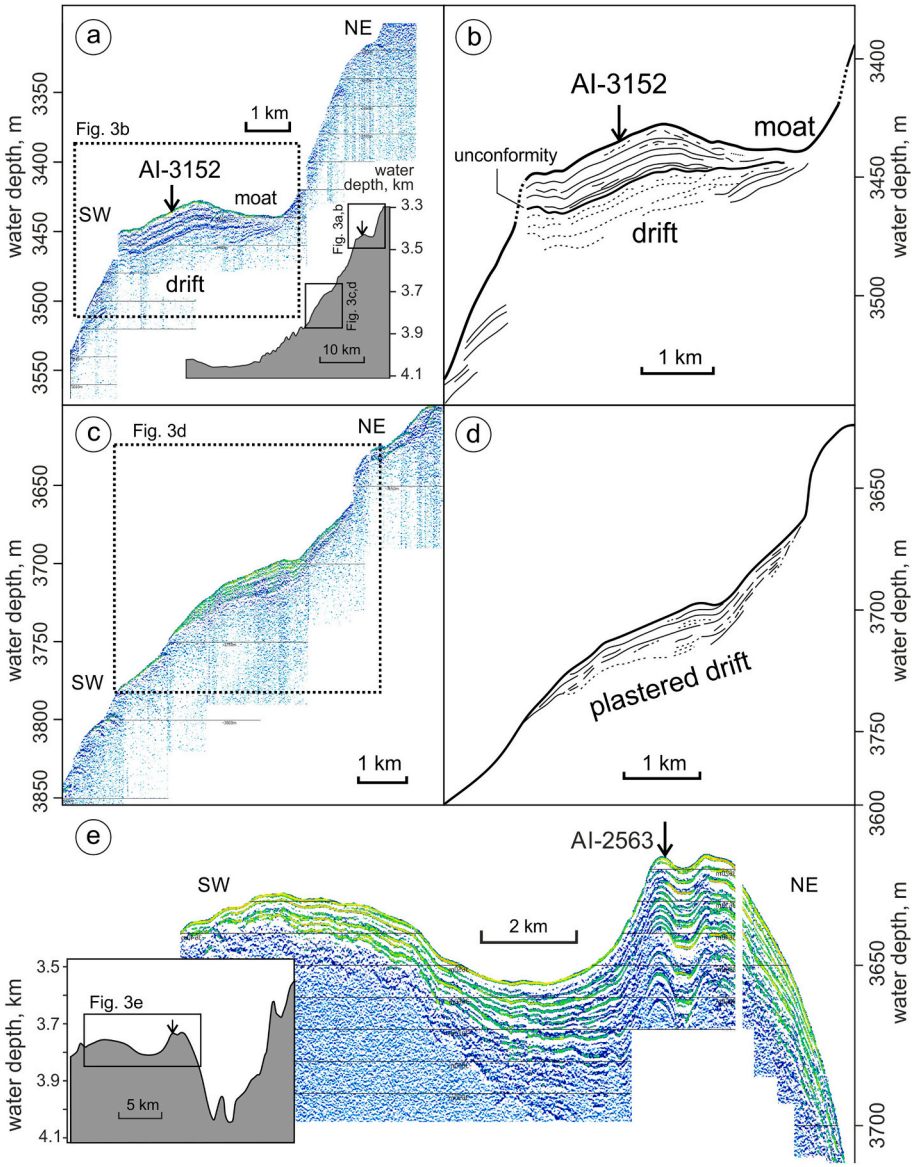

Fig. 3. Seismoacoustic structure of the upper sediment cover on the São Paulo Plateau southern escarpment and its base. Black arrows mark the location of sediment core sites.

The drifts were recorded only in one sub-bottom profile so their estimated extension along the slope can hardly exceed 40 km (Figs. 3a-d, 2a).

The main part of the SCP is covered by a low mounded, N-S elongated body (approximately 200 km long by 50 km wide), known as the Santa Catarina Drift (Fig. 1a). Analysis of sub-bottom profiling data collected on the SCP allowed distinguishing irregular, hyperbolic, distinct and undulated types of seismic facies. The distribution of these facies is generally described by Frey et al. (2022). This work is mainly focused on the undulated seismic facies (sub-type 4F) which occupy the major part of the northern Santa Catarina Plateau (Table 2). These facies are acoustically stratified seismic characters with parallel to subparallel, moderate amplitude, and continuous reflectors. The acoustic penetration varies from 40 to 70 m (Figs. 3a,e, 4). Over most of the SCP the reflectors show slight to more marked undulations (Fig. 4a-f). Some of these are regular and appear to be giant sediment waves (Fig. 4f). The lowest amplitude waves (<2 m) occur over the crest of the Santa Catarina Drift (Fig. 4e), and as part of a buried wave field (Fig. 4b), which was previously described by Borisov et al. (2020). Sediment waves with heights of 7–25 m cover the major part of the Santa Catarina Drift (Fig. 4a, b, d). The highest amplitude waves (up to 70 m) are located on the slopes of Torres High (Fig. 4f). The buried part of the sediment wave field is presented by facies 1 L. This facies type has distinct and uniform bottom echo, undulated disrupted sub-bottom reflectors, sub-parallel to each other but not to the bottom reflector.This facies alternates with 1G and 4F facies (Table 2).

The Ioffe CDS lies to the northeast of the exit to the Vema Channel. The Ioffe Drift itself drapes over a narrow tectonic ridge along the southern margin of the Florianopolis Fracture Zone, with a fault-controlled channel (or moat) along its northern flank (Fig. 2b). This fault- drift extends for up to 500 km in a northeasterly direction. There is a marked unconformity that lies about 20–40 m from the surface of the drift. Overlying this, much of the drift shows an acoustically stratified seismic character with parallel to subparallel, moderate amplitude, continuous reflectors, and a lack of reflector undulations (Fig. 5a-c, e). Some parts are less clearly stratified to nearly transparent, with some intercalation of seismic units with different amplitude of reflectors (from almost acoustically transparent to well-stratified)(Fig. 5). In places, these seismic units are separated by an angular unconformity (Fig. 5b,c, e). A series of irregular sediment waves (up to 20 m amplitude) with the

Table 2
Seismic facies (echo-character) types and subtypes revealed in the study area (with description and interpretation). Subtypes nomenclature marked with star (*) corresponds to classification by Damuth and Hayes (1977), the rest – to classification by Maestro et al. (2021).

Sub-type	SES 2000 deep example	Schematic image	Description	Interpretation
			Distinct Echos	
1G	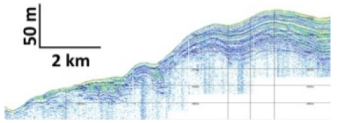		distinct and uniform bottom echo, distinct wedging out sub-bottom reflectors with acoustic blanking at the base	distinct and uniform bottom echo, distinct wedging out sub-bottom reflectors with acoustic blanking at the base
1L	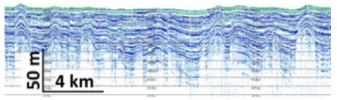	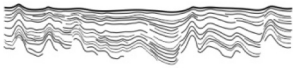	distinct and uniform bottom echo, undulated disrupted sub-bottom reflectors, sub-parallel to each other but not to the bottom reflector, acoustic penetration up to 70 m	burried/draped sediment waves
			Undulated Echos	
4F IIIB*	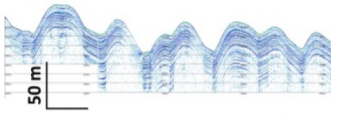	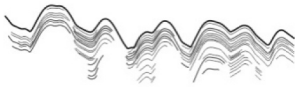	undulated bottom reflector with parallel (to sub-parallel) sub-bottom reflectors, acoustic penetration ~30 m, wave height 7-30 m, wave length 1.5-3 km	contouritic sediment waves (regular)
	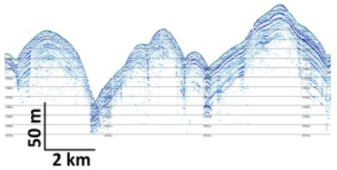		undulated bottom reflector with parallel (to sub-parallel) sub-bottom reflectors, acoustic penetration 30-40 m, wave height up to 70 m, wave length 4-5 km	contouritic sediment waves (giant)

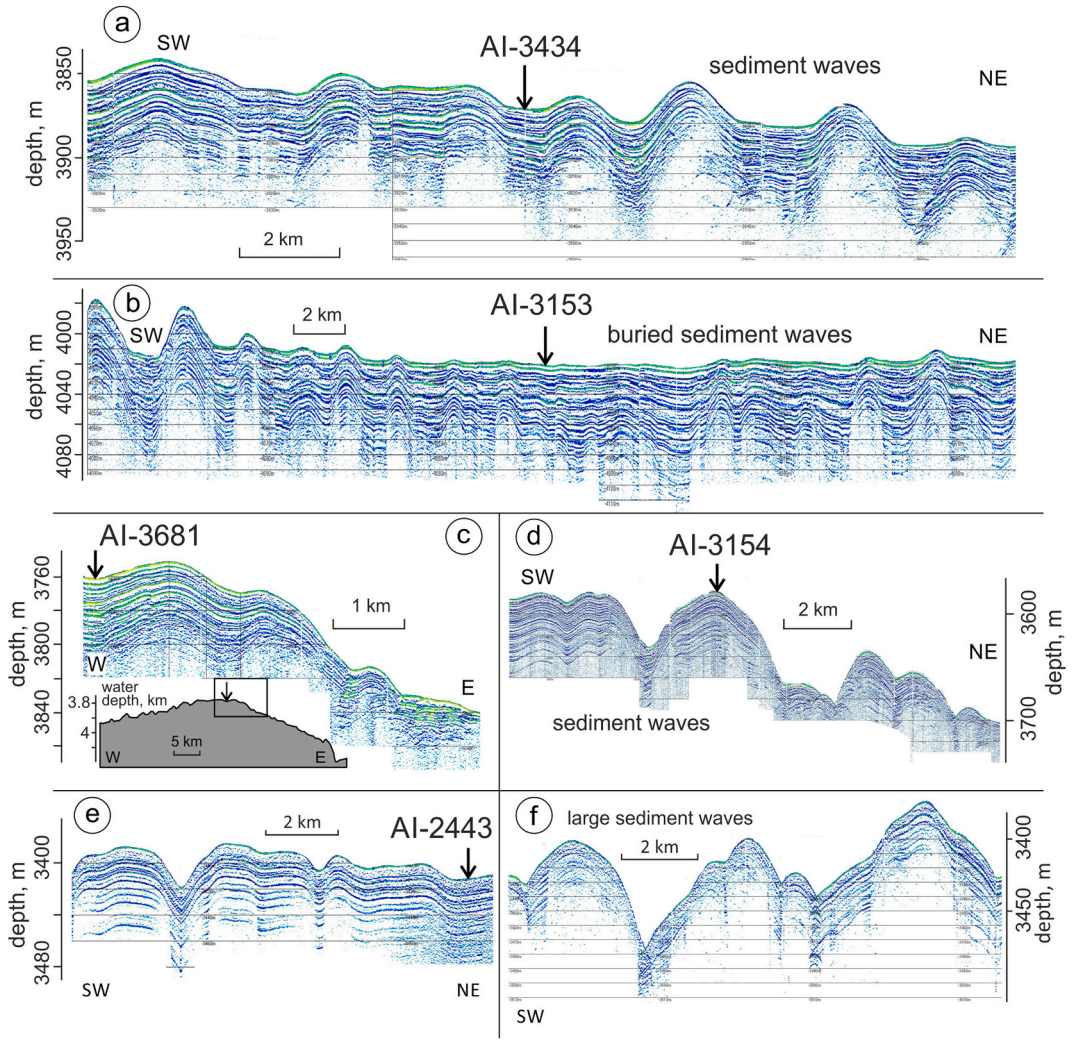

Fig. 4. Seismoacoustic structure of the upper sediment cover at core locations and examples of the sediment waves in the Santa Catarina Plateau area. Black arrows mark the location of sediment sampling sites.

same intercalation of reflective to transparent seismic units occur to the southwest of the drift (Fig. 5d).

Outcrops of some older deposits (or even basaltic basement) were revealed in sub-bottom profiling records (Fig. 5e). The mound-like outcropping features have a relative height of approximately 50–90 m and a width at the base of 2–4 km. Several well-defined moats (or scours?) were found at the base of these mounds (Fig. 5a). The relative depth of the moats (scours) varies from 5 to 40 m, while their width reaches 2 km. Notably, all the moats are located south of the mounds.

5.2. Sediment characteristics

5.2.1. The Santa Catarina Plateau – São Paulo Plateau area

According to shipboard visual core description, grain size data and geochemical data (ln(Ca/Al), all eight cores in this region (Fig. 2, Table 1) are composed of olive-gray, fine-grained sediment of mixed terrigenous-biogenic composition (Figs. 6-10). There is a relatively thick (up to 45 cm) surface oxidized brownish layer. The evidence of mixed sediment composition and the lithology of the reference cores AI-3152 and AI-2563 are described in Ovsepyan and Ivanova (2019) and Borisov et al. (2013), respectively. All cores show an interlayering of distinctive stiff mud horizons, of brownish, yellowish and bluish colors. These are especially marked in cores AI-3154, AI-3152, AI-3681, AI-2443, AI-3153 and AI-2563 (Fig. 9). Several, sharp erosional contacts are present in cores AI-3152, AI-3681, AI-3434, AI-3153, AI-3154 and AI-3435 (Fig. 9). The sediments are slightly-to-strongly bioturbated throughout the section in most cores, although in cores AI-2443 and AI-3153 only part of the section appears bioturbated (Fig. 7). In some cases, sediment lamination is also present, as in cores AI-3434 (18–26 cm) and AI-3681 (34–46 cm).

Detailed grain size analysis shows a dominance of silt and clayey silt, with a sandy silt and sand fraction only present in thin layers in cores AI-3435, AI-3152, AI-3434 and AI-3681 (Figs. 7-10). The mean grain size of the bulk sediment is low throughout much of the core sections (typically in the range 2–20 μm), but with distinctive intervals extending over 10–50 cm in which the mean grain size increases markedly (up to 50–400 μm). In some cores (e.g. AI-3153 and AI-3154), the coarser intervals are fine to coarse silt, whereas in others the mean grain size is fine to medium sand (e.g. AI-3435 and AI-3152). Sediment sorting is mostly very poor (> 2 phi), but some of the coarser intervals show improved sorting (< 2 phi). This trend is very clear in core AI-3435, for example, but the reverse is true for some other cores – e.g. AI-3154.

These bi-gradational sequences are also evident in the down-core plots of ln(Ca/Al) (Fig. 9). The higher ln(Ca/Al) tend to correspond with coarser mean grain sizes, although this is not everywhere evident. In some cases, the coarser fraction is dominated by planktic foraminiferal tests and their fragments, whereas in other cores this fraction is mostly terrigenous (Fig. 8). The ln(Ca/Al) ratio is generally lower in the

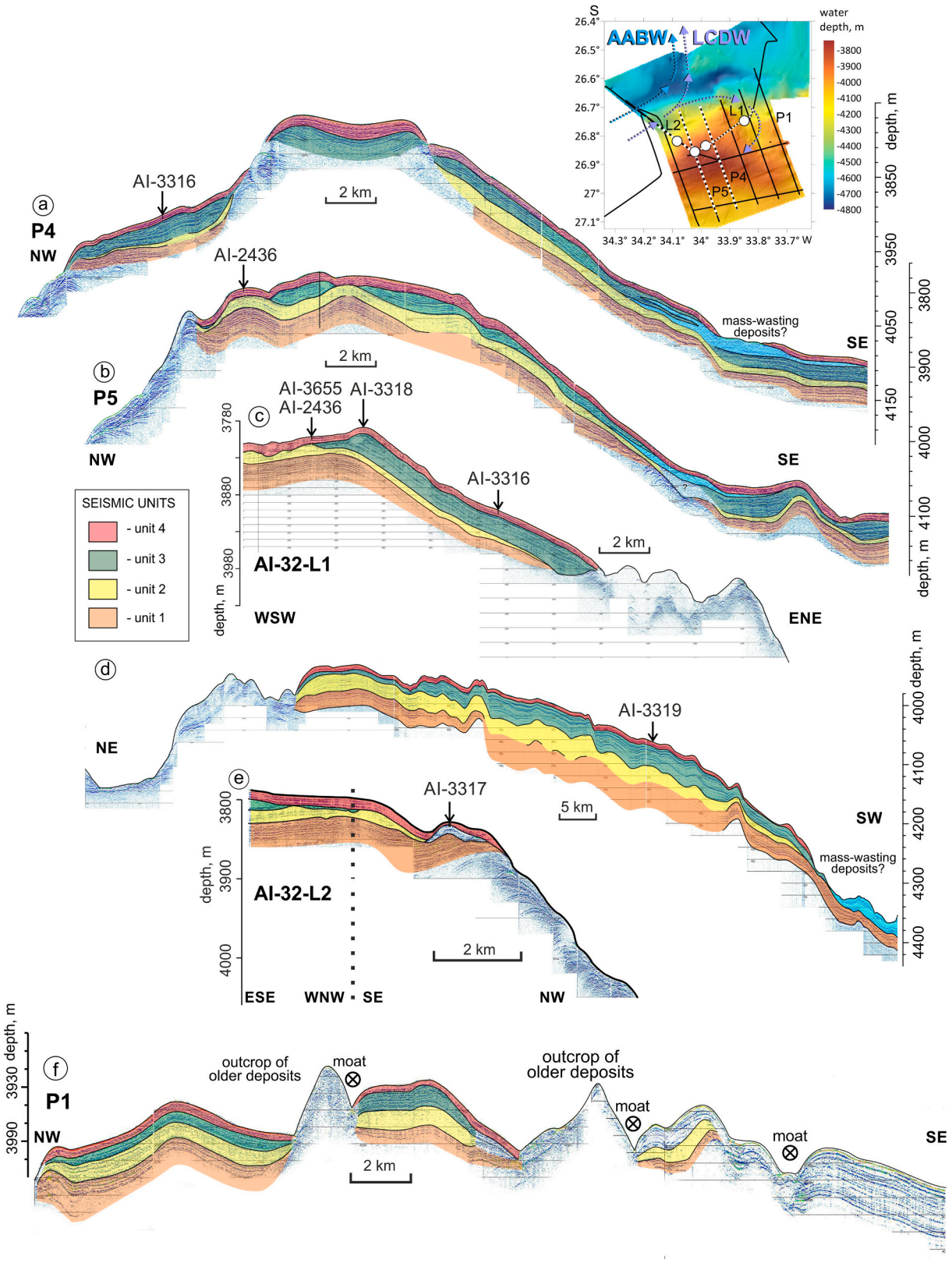

Fig. 5. Seismoacoustic structure of the upper sediment cover in the area to the southwest of the Ioffe Drift. Black arrows mark the location of sediment sampling sites.

finer-grained sections, but increases in the coarser intervals. It is also seen to vary between cores across the Santa Catarina Plateau – São Paulo Plateau area (Fig. 9).

The *SS* mean size generally varies between 11 and 40 μm reaching up to 53 μm in the coarse layers from core AI-3434 (Fig. 10). In cores AI-3434, AI-3681 and AI-3153, several layers are characterized by an absence of clay, thus the whole terrigenous fraction <63 μm consists of a sortable silt fraction. The ratio of *SS* content to its mean size shows very high correlation coefficients (0.91–0.98) in all cores studied (Fig. 8).

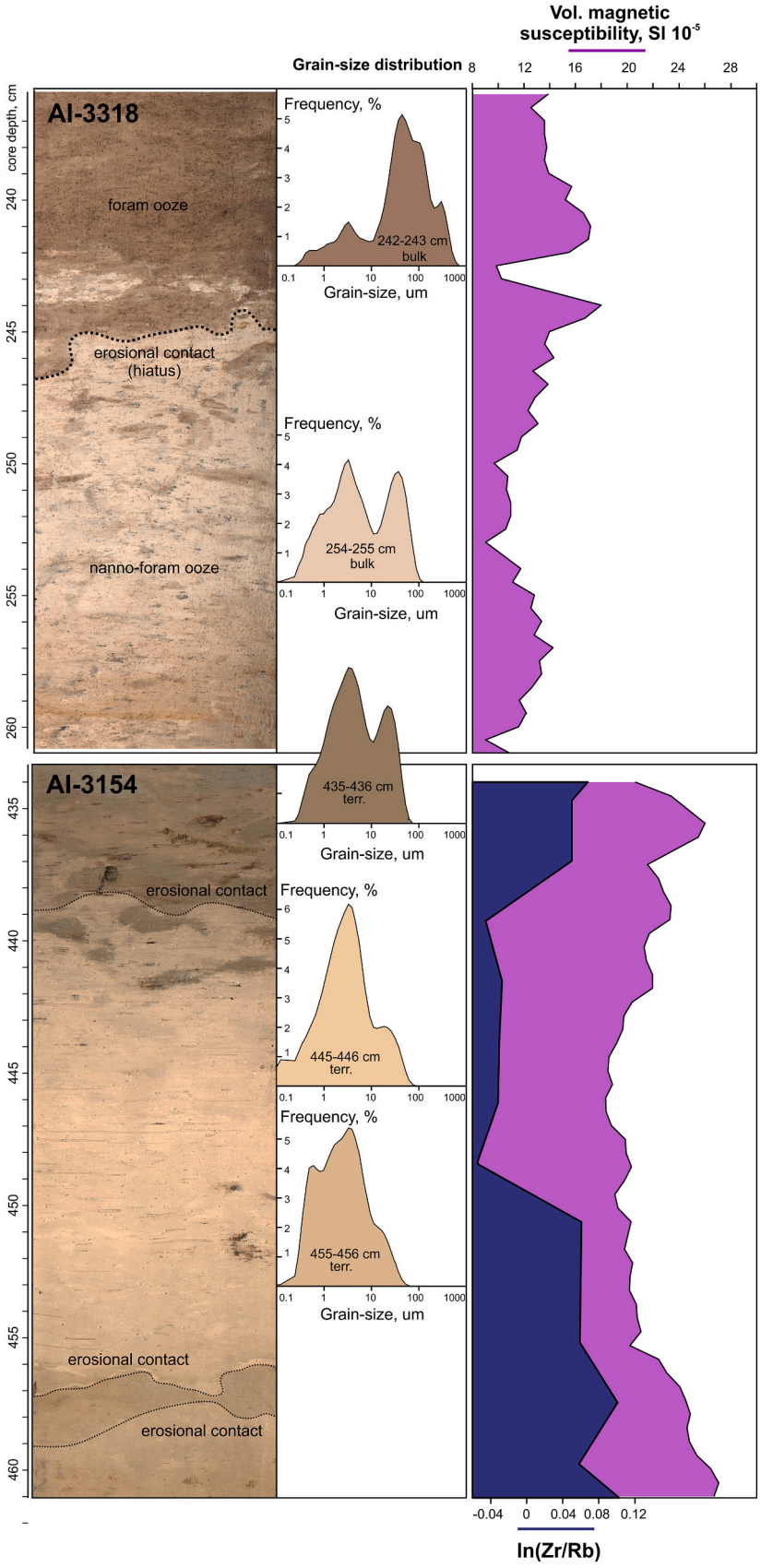

Fig. 6. High-resolution images of cores AI-3318 (Ioffe Drift) and AI-3154 (Santa Catarina Plateau) with interpretation, grain-size distributions, volume magnetic susceptibility (magenta) and ln(Zr/Rb) ratio (dark blue). (For interpretation of the references to colour in this figure legend, the reader is referred to the web version of this article.)

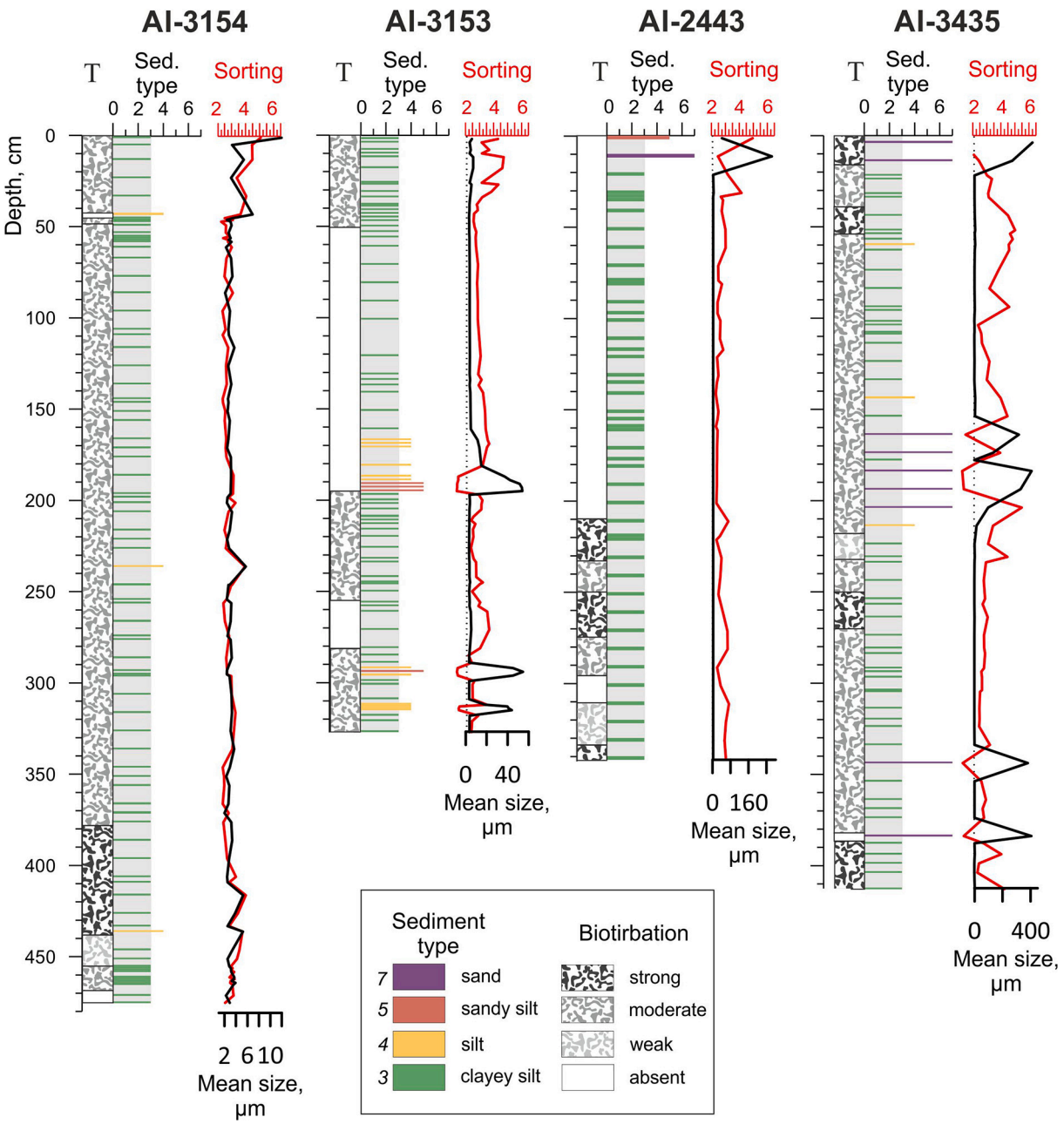

Fig. 7. Sediment cores from the Santa Catarina Plateau – São Paulo Plateau area: sediment structures, sediment types distribution, sorting and mean size of the bulk sediments versus depth.

5.2.2. *The Ioffe Drift –Rio Grande Rise area*

5.2.2.1. Ioffe Drift. All six sediment cores from the Ioffe Drift area recovered very pale brown to pale orange-yellow bioturbated calcareous ooze, mostly composed of planktic foraminiferal tests (whole and fragmented) and calcareous nannofossils (Figs. 6 and 11; see Fig. 2b and Table 1 for locations). Nannofossils dominate in the lower parts of cores AI-3317 and AI-3319, where the sediments are represented by nannofossil ooze and the strongest foraminiferal dissolution is documented (Ivanova and Dmitrenko, 2021; Murdmaa et al., 2021a). However, a slowdown of the bottom currents could also result in the relative coccolith accumulation along with the dissolution. Foraminiferal ooze is present in the upper 10–40 cm of most cores, and at discrete intervals down-core. The relative proportion of biogenic to terrigenous material varies laterally, from core to core, and vertically down-core. The terrigenous fraction content is generally higher in core AI-3319 compared to the other cores. However, brownish-colored layers (up to several centimeters in thickness) enriched in terrigenous material also occur in core AI-2436 (Murdmaa et al., 2021a).

Detailed grain size analysis shows subtle differences between cores (Figs. 11, 12). There is a dominance of silt and clayey silt in cores AI-3319, AI-3316 and AI-3317 (pre-drift and drift flank), sandy silt in core AI-3655, and more silty sand to sand-size in cores AI-2436 and AI-3318 (drift crest) (Fig. 12). The bulk mean grain-size varies from around 10 μm in the nannofossil oozes (e.g. AI-3317) to almost 250 μm in foraminiferal sand intervals (AI-3318). Sediment sorting is generally very poor, with a sorting coefficient up to 7 phi (Fig. 11). Down-core oscillation of both mean grain-size and sorting parameters is evident in all cores, being more pronounced and variable in the generally coarser-grained cores (e.g. AI-3318). This is comparable with the bi-gradational sequences noted in the Santa Catarina region above.

Because the Ioffe Drift sediments are so rich in $CaCO_3$, we could not

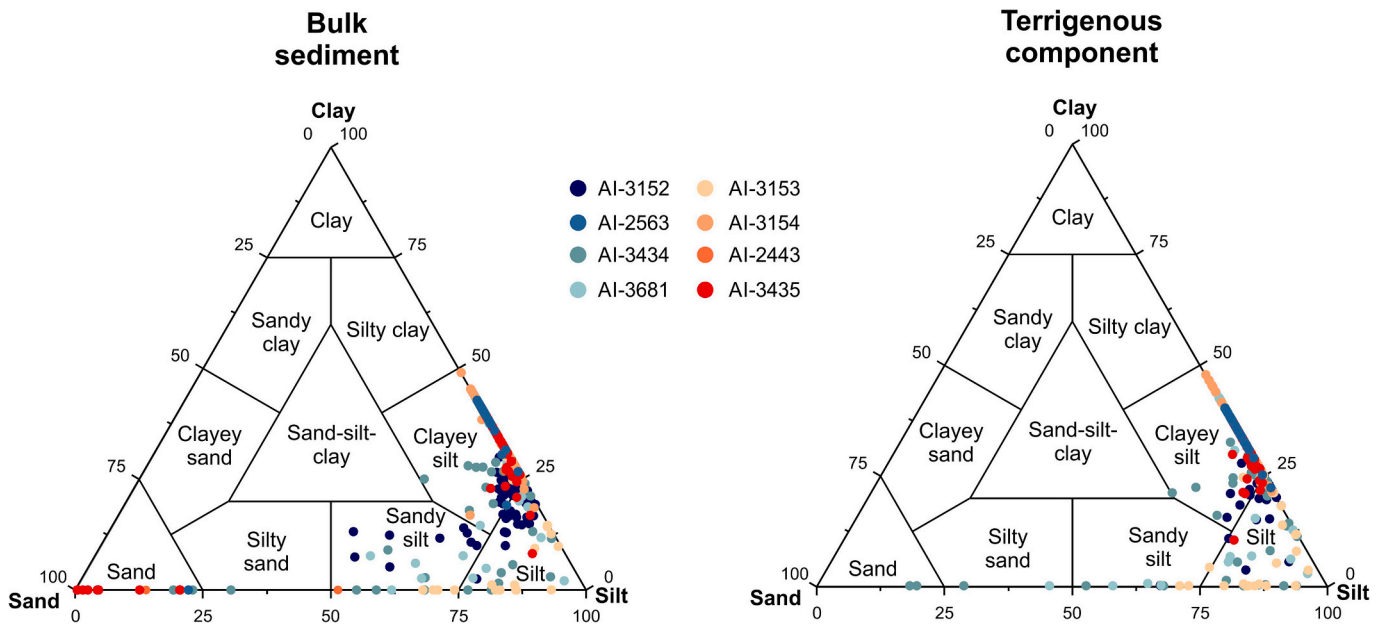

Fig. 8. Ternary diagrams (according to Shepard, 1954) of the grain-size distribution in the sediment cores from São Paulo Plateau – Santa Catarina Plateau area.

measure a *true* sortable silt proxy, following the removal of the carbonate fraction. However, we calculated an *equivalent SS* measure (i.e. mean of the bulk 10–63 μm fraction) and cross plot this with the bulk mean size. The correlation coefficients range from 0.78 to 0.89 for four drift cores, with somewhat lower values (0.59 and 0.69) for cores AI-3317 and AI-2436 from the northern slope and summit of the drift, respectively (Fig. 13). The maximum value of 0.89 is estimated for core AI-3319, retrieved from the field of the sediment waves to WSW of the Ioffe Drift (Fig. 13A).

One grab sample (AI-3654) recovered a 20 cm-long section of terrigenous clayey silt from the northern slope of the fault-controlled channel at the base of the northern flank of the Ioffe Drift, at a water depth of 4695 m (Fig. 12). Several ferromanganese nodules are found on the sediment surface in this grab. The sediments are slightly bioturbated in the lower part of the section. Two further grabs attempted from the deepest part of the channel, at water depths of 4700–4770 m, were returned empty.

5.2.2.2. Rio Grande Rise. Two cores were recovered from the Rio Grande Rise, southwest of the Ioffe Drift (Table 1). The sediments of a short core (AI-3320) from the summit of Rio Grande Rise consist of relatively poorly sorted foraminiferal sand (Fig. 11), whereas a deeper and longer core (AI-3321) collected from the rise' slope recovered an alternation of foram-nannofossil and nannofossil-foraminiferal oozes. A conspicuous amount of pteropod shell fragments and perfectly preserved planktic foraminiferal tests are present in both cores. Grain-size analysis shows the dominance of sand fraction in all samples studied from both cores (Fig. 12). The ratio of the *equivalent SS* content in the fraction <63 μm to *SS* mean size demonstrates a high correlation coefficient of 0.9 in core AI-3321 and a very low coefficient of 0.3 in core AI-3320 (Fig. 13).

5.3. Stratigraphy and sedimentation rates

5.3.1. AMS ^{14}C dating

Ten new calibrated AMS ^{14}C dates are presented in this study, as well as five previous dates from the region (Table 3). Together, these ages range from around 31 ka to 4.8 ka, and so help calibrate the late Quaternary stratigraphy – Marine Isotope Stages (MIS) 1–3. In the Santa Catarina Plateau-São Paulo Plateau area, the dates confirm the age of the uppermost sediments within MIS 1–2. The two dates from core AI-3320 on the Rio Grande Rise clearly demonstrate an age inversion, yielding an age of 42 ka at a core depth of 5–6 cm, and an age of 27.35 ka at a depth of 25–26 cm. These cannot be used to calibrate the age of this core, but the possible reason for this inversion is discussed later. In the Ioffe Drift area, core AI-3318 yielded two dates – an age of 33.14 ka at a depth of 10–11 cm, and age of >46 ka at a depth of 20–21 cm. This last is beyond the maximum age for an accurate measurement, but interestingly, both dates show relatively older sediments (MIS stage 2) quite near the surface. Where possible the ages obtained have been used to calculate mean sedimentation rates using linear interpolation between calibrated AMS ^{14}C dates for the upper parts of cores. Otherwise, sedimentation rates have been estimated within the stratigraphic intervals identified basing on biostratigraphy, as described below.

5.3.2. The Santa Catarina Plateau – São Paulo Plateau area

In the São Paulo Plateau – Santa Catarina Plateau area, core AI-3152 from a small patch drift is used as the reference core. Its stratigraphy is based on a closely-spaced benthic oxygen isotope record, supported by AMS ^{14}C dating for the upper part (Ovsepyan and Ivanova, 2019). This core recovered the last 167 ky of a section, that is from MIS 6 to MIS 1, and yields estimated average sedimentation rates from 1.5 to 4.1 cm/ky within different MIS stages. The other seven cores from the area can be correlated to AI-3152 using the down-core ln(Ca/Al) records supported by the available AMS ^{14}C dates in four cores (Table 3, Fig. 9). The interglacial (MIS 1 and 5) and interstadial (MIS 3) periods are characterized by higher ln(Ca/Al) than the glacial/stadial periods, although the difference is more muted in cores AI-2443 and AI-3154 (Fig. 9). The stadial periods MIS 2 and 4, with relatively low ln(Ca/Al), are recovered in seven cores whereas glacial period MIS 6 is seen in three cores (Fig. 9). The average sedimentation rates vary from 0.7 to 9.1 cm/ky, and show a generally lower rate of 0.7–3.0 cm/ky for the interglacial periods (MIS 1 and 5) than for the glacial period (MIS 2–4), which ranges 2.0–9.1 cm/ky across the core sites.

5.3.3. The Ioffe Drift – Rio Grande Rise area

The stratigraphy of the Ioffe Drift is based mainly on the biostratigraphy of planktic foraminifers and nannofossils, and spans the late Pliocene to Recent (Fig. 14) (Ivanova et al., 2016a, 2020; Ivanova and Dmitrenko, 2021). This shows a much reduced succession compared

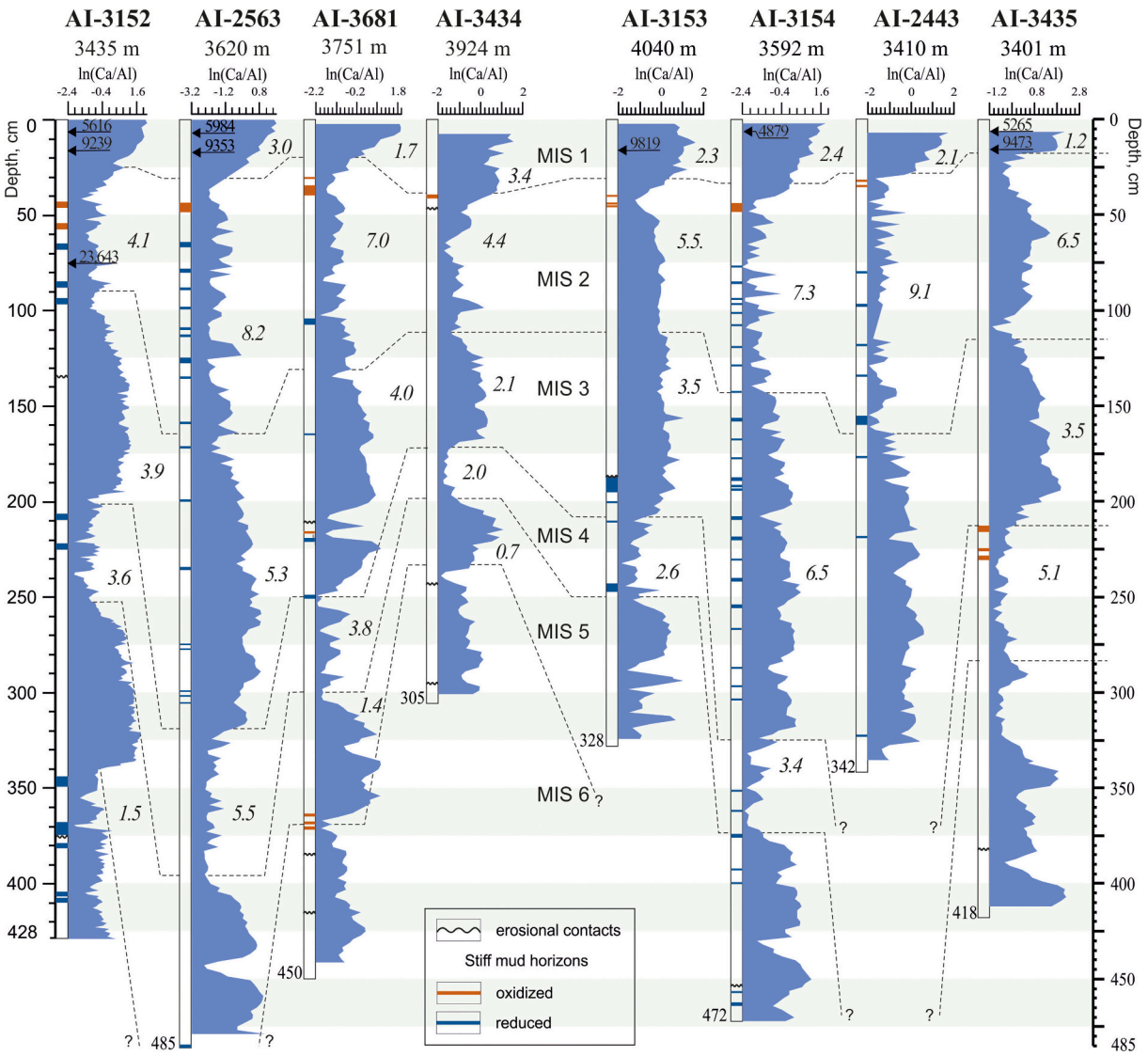

Fig. 9. Correlation of sediment cores from the Santa Catarina Plateau – São Paulo Plateau area versus the reference core AI-3152 with the established marine isotope stages (MIS, after Ovsepyan and Ivanova, 2019) based on the down-core ln(Ca/Al) records. Calibrated AMS ^{14}C dates are marked by black flash (see Table 3).

with DSDP Site 516 on the Rio Grande Rise. Correlation between the Ioffe Drift cores and DSDP Site 516 demonstrates the reduced thickness of all biostratigraphic zones, as well as the absence of some zones thus suggesting a common occurrence of erosional hiatuses in the drift area (Fig. 14). For every erosion event, the resulting biostratigraphic gap might span several tens or even hundreds thousand years (Ivanova et al., 2021).

The previous studies revealed that specific variation patterns in MS and XRF (ln(Ca/Al)) records correspond to distinctive irregular bioturbated contacts between dark brown layers relatively enriched with terrigenous material and underlying light layers with relatively higher carbonate content (Ivanova et al., 2021). These patterns represent strongly asymmetric (an abrupt change followed by a gradual one) and probably mark incomplete sedimentary cyclites, reflecting fluctuations of bottom-current velocity as described by Stow and Faugères (2008). Correlation of MS and XRF data with high-resolution linear scan images and biostratigraphic data allowed interpretation of abrupt changes in MS and ln(Ca/Al) values within the patterns described above as evidence of hiatuses (Fig. 15; Ivanova et al., 2020, 2021).

The hiatuses appear to be especially common in the Gelasian, from ~2.59 to ~1.9 Ma, based on MS-XRF records, and more evident in the Calabrian, from ~1.47 to 0.81 Ma, based on biostratigraphic data (Fig. 15). Although the age resolution does not allow an accurate estimate of the vanished stratigraphic time interval, we suggest that many of the erosional and non-depositional hiatuses are relatively short, even geologically instantaneous (Ivanova et al., 2021; Murdmaa et al., 2021b). For hiatuses within a standard contourite sequence in the Gulf of Cadiz, demonstrate a probable duration of 0.5–1.5 ky.

Cores AI-3320 and AI-3321 from the Rio Grande Rise extend back to MIS 5 and MIS 8, respectively, according to the oxygen isotope record from AI-3321 and core-to-core correlation using the ln(Ca/Al) records (Fig. 16). The interglacial and interstadial periods are generally characterized by higher ln(Ca/Al) and lower MS values. The estimated average sedimentation rates within different stages range from about 0.6 to 1 cm/ky, which is consistent with the mean value of 0.5 cm/kyr for the upper 10 m of DSDP Site 516.

6. Discussion

Overall, our data suggest that the narrow Vema Channel significantly modulated the energy transferred by bottom currents linked to the LCDW and AABW, and markedly affected sediment erosion and deposition at and near its northern exit. Thus, in line with the earlier publications on the Vema contourite fan (Mézerais et al., 1993; Faugères

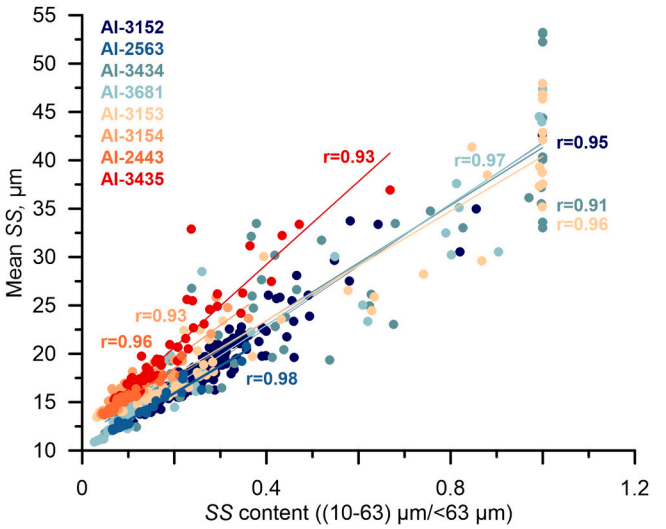

Fig. 10. Graphs of the terrigenous *SS* content in the fraction <63 µm versus *SS* mean size for the samples from the Santa Catarina Plateau – São Paulo Plateau area.

et al., 2002), we argue that this gateway is of primary importance for CDSs formation in the study area, which is mostly bathed by LCDW. Contourite deposition and erosion are also affected by the temporal and spatial variability of bottom currents in the Vema Channel (Johnson, 1984).

6.1. *Multi-proxy evidence for contourites*

The recognition of contourites and their distinction from other deep-water sedimentary systems is not always straightforward. A three-scale approach for the identification of contourites was introduced by Lovell and Stow (1981) and this is now generally accepted (Stow et al., 2002; Rebesco et al., 2014; Stow and Smillie, 2020). This method clearly acknowledges the need to consider all evidence at the large scale (oceanographic and tectonic setting, sedimentary/seismic system), at the medium scale (depositional body, morpho-seismic features); and at the small scale (sedimentary characteristics in the field, cores and through laboratory analysis). Following this methodology, there is strong evidence at the *large scale*, from the physiographic and oceanographic setting of the region (see Section 2), for a regional context that would favor contourite accumulation from at least Oligocene time. This is fully supported by many previous studies of the Vema Channel and associated drift deposits (Johnson et al., 1984; Ledbetter, 1986; Mézerais et al., 1993; Faugères et al., 2002; Jeck et al., 2019). Observations at the *medium scale* (morpho-seismic features) and *small scale* (sedimentary characteristics), which further support a contourite interpretation, are discussed separately below for the two study areas: the Santa Catarina Plateau – São Paulo Plateau, and the Ioffe Drift – Rio Grande Rise.

6.1.1. *The Santa Catarina Plateau – São Paulo Plateau area*

6.1.1.1. Morpho-seismic features. Sediment waves covering the Santa Catarina Plateau are recorded in seismoacoustic profiles as a series of slightly overlapping hyperbolae with conformable sub-bottom reflectors. This type of acoustic (seismic) facies corresponds to type IIIB echocharacter of Damuth and Hayes (1977) or type B2 of Loncke et al. (2009). In both cases, these are taken to reflect the significant impact of bottom currents on sedimentation. We agree with this interpretation of the Santa Catarina waves, although we do accept that other mechanisms of wave formation are also possible (Wynn and Stow, 2002). Cores were recovered from different parts of these sediment waves.

According to classification by Rebesco (2005) and Hernández-Molina et al. (2008), the depositional body on the São Paulo Plateau escarpment (with its mounded overall geometry, presence of a moat, estimated along-slope elongation) can be interpreted as a separated mounded or patch drift (Fig. 3a, b). The units distinguished in the acoustic structure of the shallower drift (depth ~ 3450 m) reflect two stages of its formation. The lower unit is considered to be a small plastered drift deposited on the escarpment of the São Paulo Plateau. The reflector configuration within the unit (i.e. increased slope angle gradients) demonstrates that the drift growth modified the slope morphology. The upper unit corresponds to the formation stage of the moat and slightly mounded drift. Sub-bottom profiling data show the migration of the moat-drift system toward the escarpment. The configuration of the moat and drift together with the direction of the Coriolis force suggest the eastward movement of the bottom current. In the lower unit, the evidence of moat formation could be destroyed by erosion marked by unconformity between the two units. The event of drastic erosion was most probably caused by the intensified bottom currents. Since the shallower drift is located slightly below the modern NADW/LCPW boundary, it can be assumed that internal waves (internal tides) could increase the erosional impact on the drift and the escarpment due to the vertical migration of the boundary in the geological past. These processes probably could also contribute to the formation of terrace-like slope irregularities on the escarpment representing the substrate for the subsequent deposition of the shallower drift (e.g. Hernández-Molina et al., 2010; Preu et al., 2013).

The acoustic structure of the deeper drift (depth ~ 3700 m) is quite similar to the lower unit of the first drift The small local depression in the upslope part of the drift marks the initiation of a moat formation (Fig. 3c,d). A small terrace-like feature of the basement served as a substrate for the drift formation in this particular part of the escarpment.

Core AI-3681 was retrieved from the N-S oriented depositional body at the foot of the São Paulo Plateau (Fig. 4c) showing an along-slope elongation, mounded geometry, and a lack of any clear downslope feeding system, which taken together allow us to interpret this feature as a separated mounded drift. However, we have no data to confirm its contourite nature.

6.1.1.2. Sediment characteristics. The range of sedimentary features observed in cores from this region also supports a contourite interpretation (Figs. 7, 9), following well-documented criteria (Stow et al., 2002; Stow and Faugères, 2008; Rebesco, 2005; Rebesco et al., 2014; Stow and Smillie, 2020). There is a general absence of primary sedimentary structures, except for some layering, thin discontinuous sandy and sandy silt lamination, sharp erosional contacts and distinct hiatuses. Bioturbation is common and ubiquitous throughout. The sediment texture shows dominance of clayey silt and silt, with localized silty sand and sand grade. Sorting is generally poor. The sediment composition is mixed terrigenous-biogenic, indicative of both supplies from the land and biogenic pelagic input. There is a bi-gradational sequence from clayey silt to sandy silt especially evident in the lower part of core AI-3153 (Fig. 7), and interpreted as long-term variations in bottom current speed and/or sediment supply. Similar bi-gradational sequences are noted in many contourite successions worldwide (Gonthier et al., 1984; Gauchery et al., 2021b). The stiff mud horizons within otherwise soft sediments found in all eight cores possibly mark hiatuses associated with winnowing and hardening of the substrate. Relative enrichment of such horizons in terrigenous coarse silt and sand revealed by smear slide examination (e.g. at 45 cm in core AI-3154 and 190 cm in core AI-3153, Figs. 7 and 9) possibly suggests an increase in bottom current intensity. The presence of the brownish bands over some of these horizons (like at ~370 cm in core AI-3681) indicates that they may represent past oxidized ferruginous surface layers buried into reduced (gray) sediments (Fig. 9). We hypothesize that other reduced (dark gray) interlayers also represent past surface layers which are reduced during diagenesis. Note

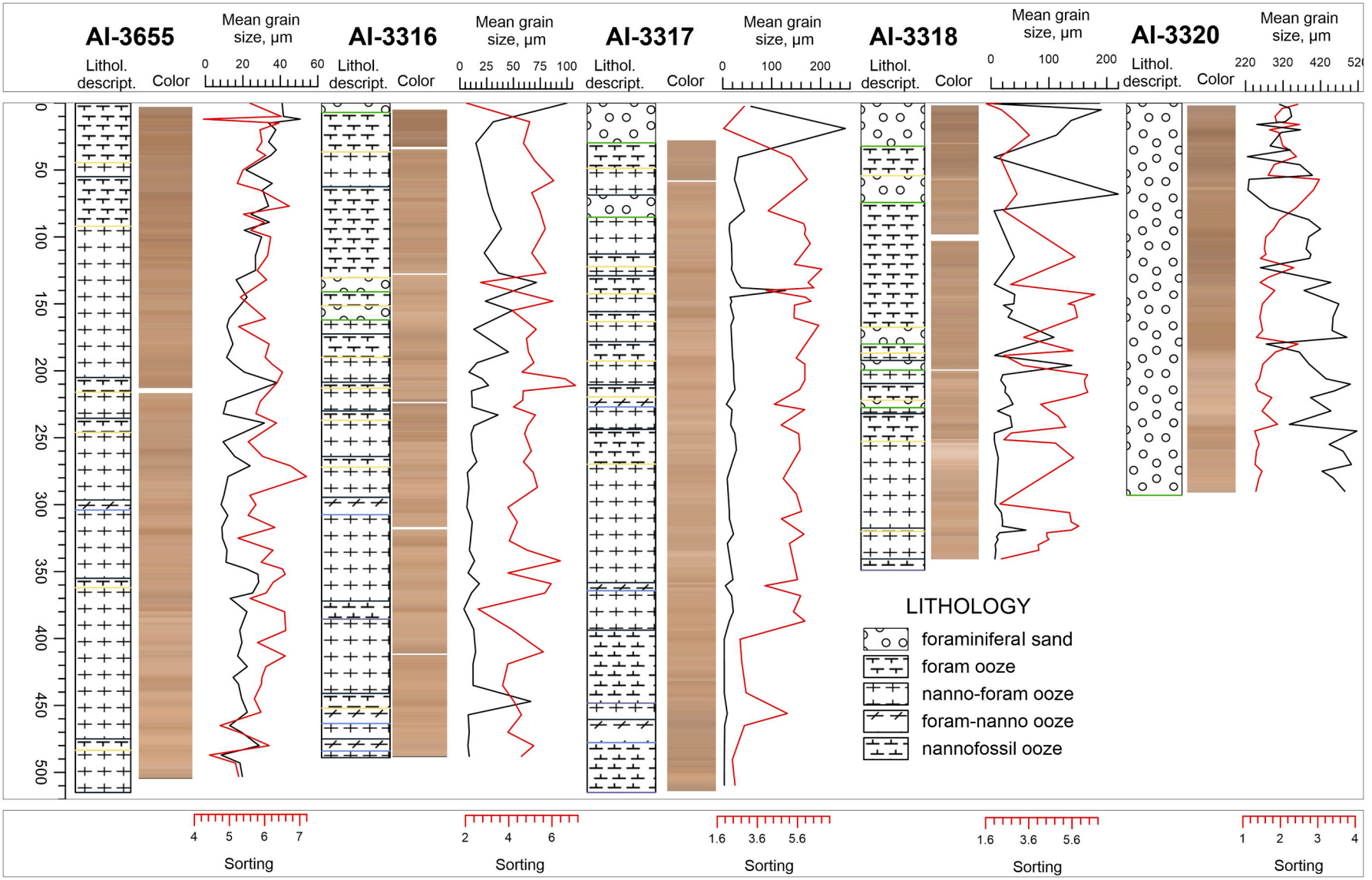

Fig. 11. Lithology, sediment sorting and mean particle size versus depth in four cores from the Ioffe Drift and core AI-3321 from the Rio Grande Rise.

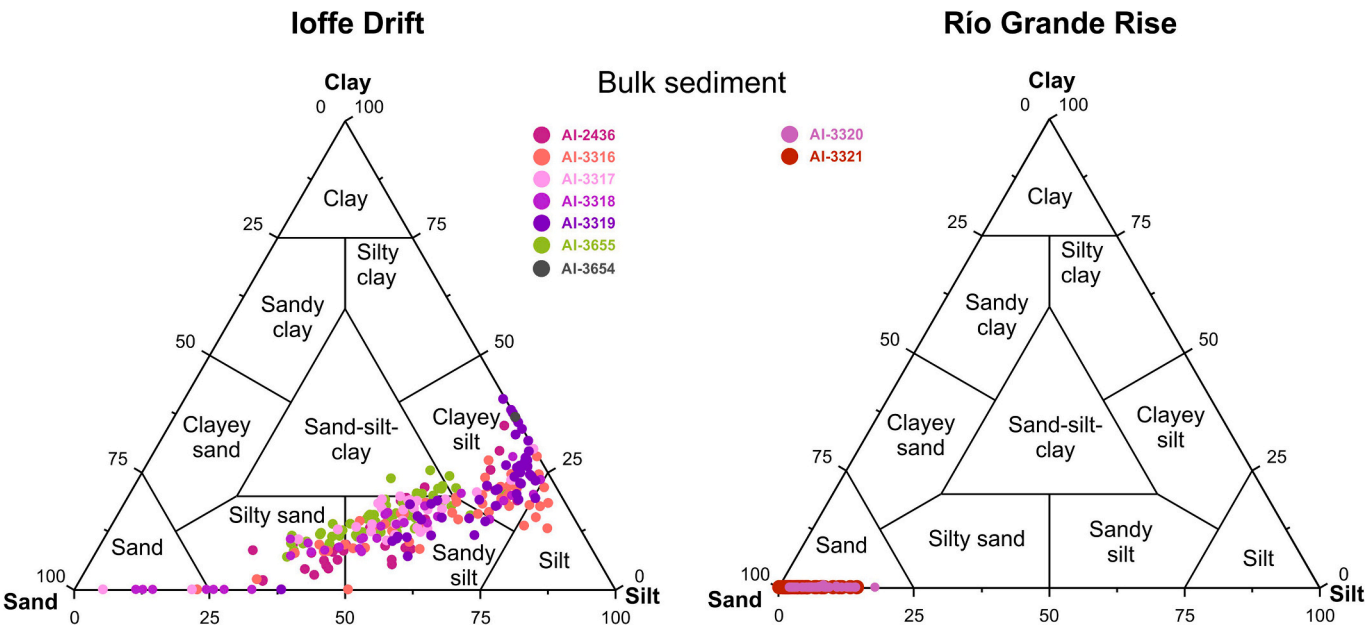

Fig. 12. Ternary diagrams (according to Shepard, 1954) of the bulk grain-size distribution in the sediment cores from (a) Ioffe Drift, (b) Rio Grande Rise.

the stiff mud horizons are characterized by cloddy texture and enrichment with sand, as present oxidized surface layers. If so, the stiff mud horizons mark episodes of slowing down sedimentation rates or even short-term hiatuses. Clay clods apparently disintegrate during ultrasound treatment of samples prior to grain size analysis and thus traces of the primary cloddy texture disappear in the analytical results.

From all eight cores studied, a very high correlation coefficient of 0.91–0.98 between *SS* content in the total < 63 μm size fraction and *SS* in the terrigenous part of sediment (Fig. 10) indicates sediment sorting by bottom currents according to McCave et al. (2017). The common presence of hiatuses, minor erosional contacts, stiff mud horizons, and intervals of very slow sedimentation or even non-deposition, are all indicative of short-term variations in depositional processes (e.g. bottom current speed), which are typical of contourite systems (Hollister and McCave, 1984; Rebesco, 2005; Stow and Faugères, 2008; McCave et al., 2017; Stow et al., 2019). Recently, the intervals of very fast contourite accumulation during the post-glacial time were documented from the shallow-water Mediterranean sites (Rovere et al., 2019; Gauchery et al., 2021b).

Although one of the sediment sources for the Santa Catarina - São Paulo Plateau CDS might be fine-grained upper suspension of turbidity currents from the Cananéia canyon, via a pirating process as invoked by several previous authors (e.g. Stow and Smillie, 2020), the terrigenous material is ultimately deposited from bottom currents as contourites. Any evidence of turbidites is absent in our cores. The distribution of turbidites from the canyon is likely restricted to a narrow fan in front of the canyon mouth, which is located far from our core sites.

The generally higher sedimentation rates during MIS 2 and 4 as compared to MIS 1, 3 and 5 (Fig. 9) suggest an enhanced bottom currents intensity during the glacials. However, this assumption is not directly supported by the grain size data which do not show a clear glacial-interglacial variability pattern (Fig. 7). Meantime, the occurrence of stiff mud horizons at the MIS 2/MIS 1 boundary (Fig. 9) pointing to the stronger bottom water hydrodynamics at the Termination I is in line with a significantly more vigorous deep Southern Ocean circulation inferred by Du et al. (2020) from the authigenic neodymium isotope records. Besides, an increase in bottom-currents speed in combination with sea level rise and consequently restricted clastics supply to the deep sea might lead to a reduced sediment accumulation in the terrigenous contourite system.

The part terrigenous composition and sedimentation rates up to 5–9 cm/ky (Fig. 9), which are higher than the norm for open ocean pelagic/hemipelagic sedimentation, possibly indicate the involvement of supply by downslope gravity processes into the sediment accumulation controlled by contour bottom currents. Similarly, an involvement of downslope processes into the contourite accumulation was previously mentioned along continental margins, e.g. in the relatively shallow parts of the Mediterranean area (Miramontes et al., 2016; Gauchery et al., 2021a, 2021b). In addition, the climatically-controlled biogenic component seems to be diluted by the terrigenous one in parts of the section, which is consistent with the water depth above the calcite saturation depth (at 3750 m in the area according to Chung et al. (2003) for most of the cores studied (Table 1). Terrigenous supply may include significant river discharge from the La Plata (Krastel et al., 2011; Razik et al., 2013; Perez et al., 2016) and Rio Doce (Gingele et al., 1999) rivers. At present, these river mouths are 1100–1460 and 1000–1300 km away from the SCP, respectively. The material from the Rio de la Plata is supposed to be transported by LCDW and AABW, whereas terrigenous sediments from the Rio Doce seem to be supplied by SACW and TW along the coast to the south and by the recirculated branch of AAIW to the deep sea areas (Fig. 1a).

Sedimentation rates are higher in the southern cores (AI-3435, AI-2443 and AI-3154) than from the northern cores (AI-3153, AI-3434, AI-3681 and AI-3152). The southern region is also noted for the occurrence of giant sediment waves (Borisov et al., 2020) suggesting active bottom-water hydrodynamics. Oceanographic measurement and modeling show bottom current speeds up to 30 cm/s, with variable directions (Frey et al., 2018; 2022), in this area. This is compatible with local erosion, hiatuses and sandy/silty intervals, as well as with sediment wave formation.

Furthermore, the initial basement highs and depressions underlying the muddy sediments in the southern part of the Santa Catarina Plateau (Jeck et al., 2019) might favor the spatial heterogeneity of bottom currents in terms of their speed and direction (e.g. Merrifield et al., 2001; Maldonado et al., 2005) thus contributing to the variability we see in the sediment record.

6.1.2. *The Ioffe Drift –Rio Grande rise area*

6.1.2.1. Morpho-seismic features. The Ioffe Drift is an asymmetric lens-

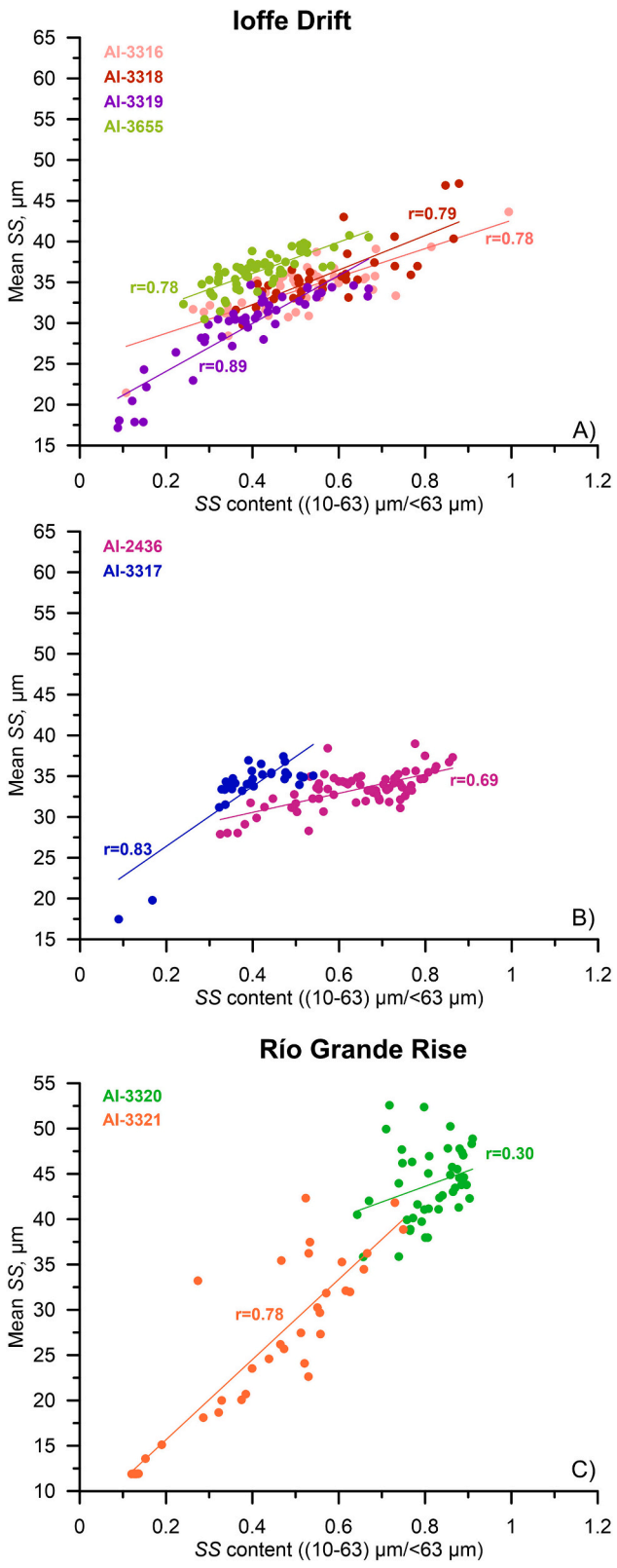

Fig. 13. Graphs of the bulk *SS* content in the fraction <63 μm versus *SS* mean size for the samples from the Ioffe Drift (a,b), Rio Grande Rise (c).

like mounded depositional body (Ivanova et al., 2016a, Borisov et al., 2021). The overall geometry, orientation, erosional and depositional features expressed in the body morphology, the shape of the seismic units, and internal unconformities indicate that the studied sediment body can be classified as a mounded contourite drift (Fig. 5). The small-scale erosional features on the drift surface (Fig. 5f) initially defined as moats (Borisov et al., 2021) can be also interpreted as scours formed around mounded outcrops of the crustal basement (or ancient deposits) under the influence of bottom currents. Scours and marginal valleys around topographic obstacles are well known and widely distributed contouritic features (Rebesco and Stow, 2001; Hernández-Molina et al., 2008; Rebesco et al., 2014; Eberli and Betzler, 2019). The velocity of the water flow increases around such obstacles and the Coriolis force deflects the flow toward the outcrop (to the left, in the Southern Hemisphere). This process resulted in the formation of such erosional features at the base of the mounded outcrops. The relative positions of the moats (south of the mounds) imply an easterly direction of the bottom current, which corresponds to the suggested direction of the LCDW current in this area (Frey et al., 2018).

Six sediment cores were retrieved from the uppermost parallel stratified unit overlying a well-defined angular unconformity (especially evident at site AI-3318) suggesting a marked erosional event. The high-resolution seismic profiles demonstrate a sediment wave field to the WSW of the drift, where core AI-3319 was retrieved (Fig. 5d), i.e. between the drift and Vema Channel.

6.1.2.2. Sediment characteristics. The sediment cores recovered from the Ioffe Drift and Rio Grande Rise are highly calcareous. The region is far from any source of terrigenous sediment (see Table 1, Fig. 1) and is therefore supplied almost entirely by pelagic biogenic material. The deeper calcite saturation depth of about 4000 m in this region, compared to ~3750 m in the Santa Catarina area (Chung et al., 2003), and the deeper foraminiferal lysocline of about 4050 m (Melguen and Thiede, 1974) also favor preservation of calcareous sediment.

However, the sediments still share many characteristics that are typical of mixed terrigenous-biogenic contourite systems (Rebesco, 2005; Rebesco et al., 2014; Stow et al., 2002; Stow and Faugères, 2008; Stow and Smillie, 2020). These include: an absence of primary sedimentary structures, common bioturbation, poor to very poor sorting, sediment layering (in some cases) and erosional contacts call on the contourite origin of the Ioffe Drift sediments. On the Rio Grande Rise, the calcareous sediments are almost completely composed of biogenic sand fraction, whereas on the Ioffe Drift summit the sediments are generally finer-grained, but with some biogenic sandy intervals. This may be due to the difference in water depth, ~ 3800 m for the Ioffe Drift compared with ~1300 m for the Rio Grande Rise (Table 1), which has affected the relative bottom current energy. In core AI-3320 from the summit of Rio Grande Rise, the strong dominance of sand fraction and better sorting reflect the action of vigorous bottom currents winnowing and removing the silt/clay fraction.

The attempt to use a modified sortable silt proxy for these carbonate-rich sediments had a mixed result (Fig. 13). The correlation coefficient between the *SS* content in the <63 μm size fraction and *SS* mean size ranges from relatively high in some cores (0.9) to very low in others (0.3). These relatively low values (0.3–0.9 or 0.69–0.9 if a shallow core AI-3320 is not taken into account, Fig. 13) compared to the terrigenous sediments from the Santa Catarina Plateau – São Paulo Plateau area (0.91–0.98) are probably a specific feature of calcareous contourites. They reflect a more constant *SS* mean size relative to more variable *SS* content in the <63 μm size fraction (Fig. 13). We argue that this finding suggests another source of *SS* fraction in the drift sediments along with its in situ setting from the nepheloid layer (commonly consisting of nannofossils) (Murdmaa et al., 2021b). It might indicate a distant transport (lateral advection) of already sorted material, mostly foraminiferal fragments of about 30 μm mean size, to the drift area. These fragments are likely transported together with nannofossils by turbulent flow from the Vema Channel or from the western slope of the Rio Grande Rise and then settle from suspension in the bottom-water layer of the LCDW gyre located above the Ioffe Drift summit (Fig. 2b). Besides, a

Table 3
Accelerator mass spectrometry (AMS) 14C dates and calibrated ages. The calibration is based on CALIB 8.2 (Stuiver et al., 2021).

Core	Laboratory code	Depth, cm	Dated material	Radiocarbon age, years	Calibrated calendar age range (±1σ), years BP	Calendar age*, years BP	Reference
Southern São Paulo Plateau area							
AI-3152	Poz-71,477	6–7	mixed planktic foraminifers	5265 ± 35	5348–5516***	5432***	Ovsepyan and Ivanova, 2019
AI-3152	Poz-79,022	16–17	mixed planktic foraminifers	8590 ± 40	8955–9134***	9045***	Ovsepyan and Ivanova, 2019
AI-3152	Poz-83,877	75–76	mixed planktic foraminifers	20,020 ± 130	22,958-23,322***	23,140***	Ovsepyan and Ivanova, 2019
AI-2563	Poz-71,474	7–8	mixed planktic foraminifers	5770 ± 35	5899–6068	5984	This study
AI-2563	Poz-79,020	17–18	mixed planktic foraminifers	8840 ± 40	9276–9430	9353	This study
Santa Catarina Plateau							
AI-3153	Poz-103,403	16–17	mixed planktic foraminifers	9240 ± 50	9694–9944	9819	This study
AI-3154	Poz-103,405	6–7	mixed planktic foraminifers	4800 ± 35	4797–4960	4879	This study
AI-3435	Poz-103,387	5–6	mixed planktic foraminifers	5110 ± 35	5167–5363	5265	This study
AI-3435	Poz-103,388	15–16	mixed planktic foraminifers	8970 ± 50	9403–9543	9473	This study
Ioffe Drift							
AI-3318	Poz-71,478	10–11	mixed planktic foraminifers	33,140 ± 580	36,138-37,582	36,860	Ivanova et al., 2020
AI-3318	Poz-71,479	20–21	mixed planktic foraminifers	>46,000	–	–	Ivanova et al., 2020
Río Grande Rise							
AI-3320	Poz-71,475	5–6	mixed planktic foraminifers	42,000 ± 2000**	42,574-45,557	44,066**	This study
AI-3320	Poz-71,476	25–26	mixed planktic foraminifers	27,350 ± 220	30,450-30,919	30,685	This study
AI-3321	Poz-71,467	10–11	mixed planktic foraminifers	13,420 ± 70	15,186-15,463	15,325	This study
AI-3321	Poz-71,468	20–21	mixed planktic foraminifers	22,050 ± 130	25,280-25,624	25,452	This study

Notes
Poz - Poznan Radiocarbon Laboratory.
* Mean value of ±1σ range.
** Age reversal (not used in the study).
*** Re-calibrated using MARINE20 calibration curve and CALIB 8.2 software.

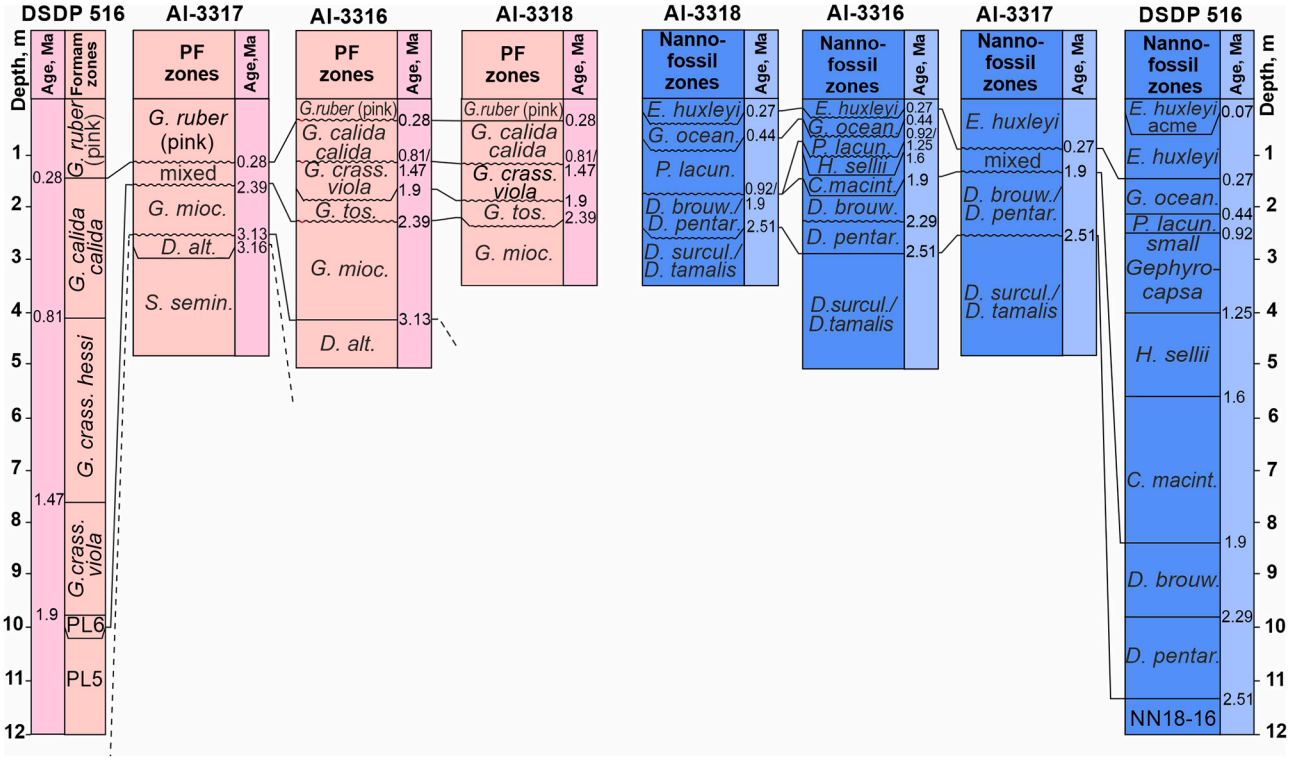

Fig. 14. Correlation of biostratigraphic zones in cores from the Ioffe Drift and DSDP Site 516 (after Ivanova et al. (2020) and Ivanova and Dmitrenko (2021) with changes and additions). In DSDP Site 516, the zonations of Barash et al. (1983) on planktic foraminifers and Dmitrenko (1987) on nannofossils are used for the upper ~10 m, while the zonation of Berggren et al. (1983a) is applied below using the zonal boundary ages from Wade et al. (2011) and Bergen et al. (2019). PF zones mean planktic foraminiferal zones. Assumed boundaries between zones and hiatuses are marked by dashed lines and undulated horizontal lines, respectively. Nominate taxa names: *G. crass. hessi (viola)* = *G. crassaformis hessi (viola)*, *G. mioc.* = *G. miocenica*, *D. alt.* = *Dentoglobigerina altispira*, *S. semin.* = *S. seminulina*, *G. tos.* = *G. tosaensis*, *G. ocean.* = *G. oceanica*, *P. lacun.* = *Pseudoemiliania lacunosa*, *C. macint.* = *Calcidiscus macintyrei*, *D. brouw.* = *Discoaster brouweri*, *D. pentar.* = *D. pentaradiatus*, *D. surcul.* = *D. surculus*.

specific shape, chemical composition and density of biogenic calcareous particles (Eberli and Betzler, 2019) might affect the correlation coefficient between *SS* content of sortable silt in the total < 63 μm size fraction and *SS* mean sizes in calcareous contourites.

We assume that after settling onto the bottom and total decay of primary organic matter the biogenic particles (foraminiferal tests and coccoliths) behave like normal terrigenous material in the bottom current field. This is not quite true for intact water filled foraminiferal tests, which are more easily moved than terrigenous sand grains of the same size. However, they are almost all fragmented in our cores and therefore likely to behave according to their size and density (2.71 g/cm^3, i.e. close to 2.65 g/cm^3 in quartz). In this case, sortable silt proxy by McCave et al., 2017should be valid for these particles also. The *SS* range from 10 to 63 μm applies only to planktic foraminiferal fragments, as the coccoliths are much smaller. In fact, the high-calcareous contourites of the Ioffe Drift have up to 50% (or more) foraminiferal test fragments of *SS* size range. They seem to be derived from sites below the lysocline and transported to the sampling sites by bottom currents. The selective deposition of fragments depending on bottom current velocities represents a typical contourite process.

Whereas mixed terrigenous-biogenic contourite drifts, notably from the North Atlantic and Mediterranean, are commonly characterized by rather high sedimentation rates (e.g. 10–115 cm/ky or even higher: Robinson and McCave, 1994; Stow et al., 2013; Rebesco et al., 2014; Miramontes et al., 2016; Gauchery et al., 2021b), this is not the case for the Ioffe Drift and Rio Grande Rise where they are generally lower than 1 cm/ky (Fig. 16), i.e. also significantly lower than in the Santa Catarina – São Paulo Plateau area (see Fig. 9).

Our new cores refine the earlier interpretation of the hiatuses distribution in the Ioffe Drift area (Ivanova et al., 2016a, 2020, 2021). Whereas the hiatuses inferred from the abrupt changes in MS values and Ca/Al ratio are mainly concentrated in the Gelassian, from ~2.59 to ~1.9 Ma, the biostratigraphic hiatuses are more typical of the Calabrian, from ~1.47 to 0.81 Ma (Fig. 15; Ivanova et al., 2021). The extensive distribution of hiatuses in the Ioffe Drift area provides a strong evidence for a contourite origin of the recovered Upper Pliocene – Quaternary sediments. Any significant impact of selective dissolution on sedimentation is considered unlikely (Ivanova et al., 2020; Murdmaa et al., 2021b). This conclusion is supported by the data obtained from the fault-controlled channel at the base of the steep northern flank of the Ioffe Drift. Here, evidence in favor of erosion by bottom currents linked to the AABW is provided by the empty grabs from the deepest part of the channel, as they most likely bounced off a hard eroded substrate, as well as by the occurrence of ferromanganese nodules found at the seafloor in grab AI-3654 from its northern slope. The nodules are also reported from cores AI-2436, AI-3316 and AI-3318 (Ivanova et al., 2016a; Shulga et al., 2021).

Along with biostratigraphic data, the AMS ^{14}C dating (Table 3) and core-to-core correlation using ln(Ca/Al) records show relatively low average sedimentation rates on the Rio Grande Rise (about 0.5 to 2.6 cm/ky, Fig. 16), at a water depth of 3000 to 1000 m, and even lower rates on the Ioffe Drift summit, at water depth of 3750–3800 m (about 0.3 cm/kyr). In turn, the correlation of ln(Ca/Al) and δ ^{18}O records from core AI-3321 is considered to be robust and consistent with the previously published correlation of %$CaCO_3$ and oxygen isotope records from core CH115–88 (Jones et al., 1984). Besides, the previous study of the giant sediment cores from the western flank of the Rio Grande Rise revealed similar values of sedimentation rates, from 0.5 to 1 cm/ky (Johnson et al., 1984). The latter seems to result from the lower erosional activity of UCDW/NADW as compared to LCDW. All these

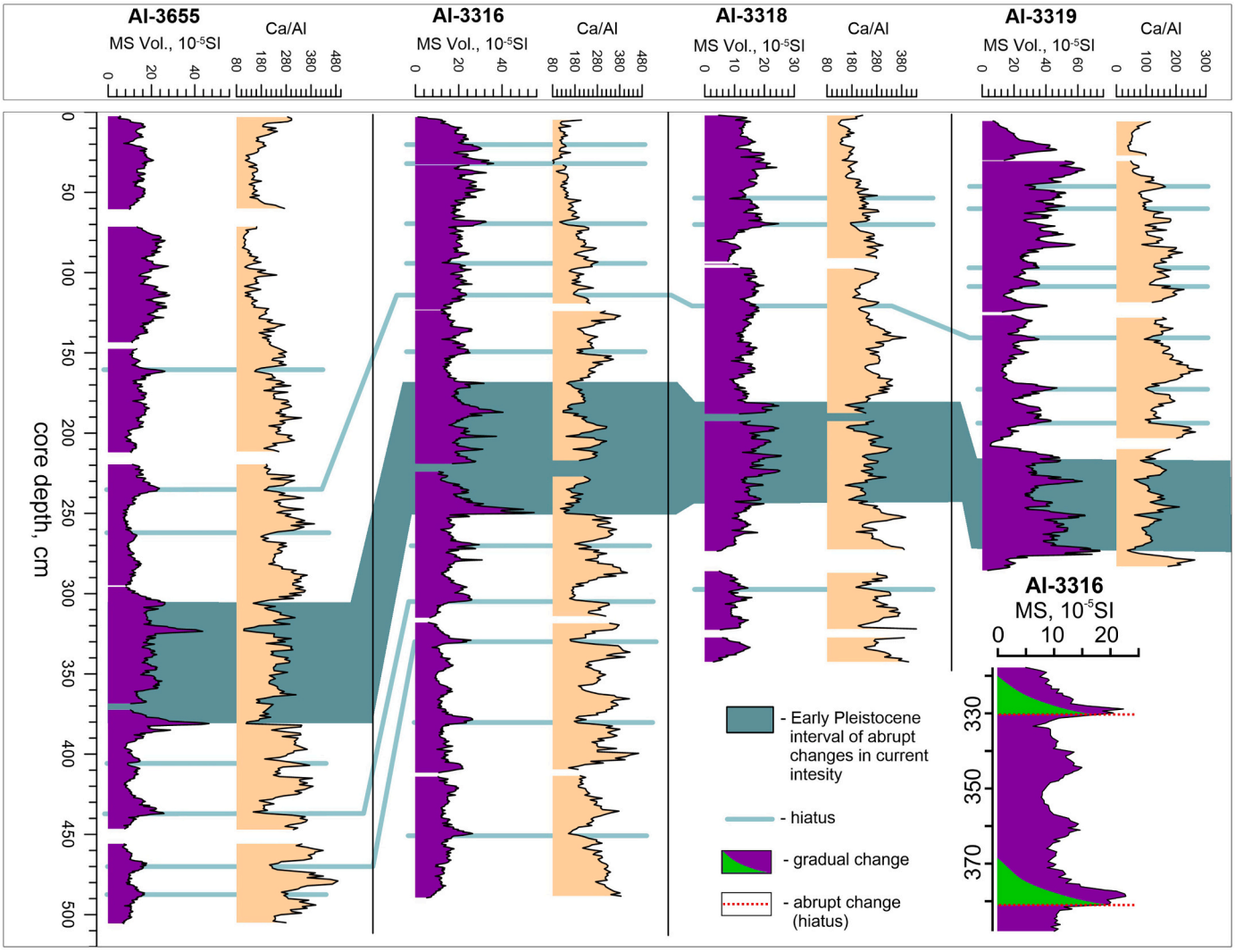

Fig. 15. Core correlation in the Ioffe Drift area based on ln(Ca/Al) and MS records and inferred hiatuses. The data are from Ivanova et al. (2020, 2021).

values of sedimentation rates are close to the values <1 cm/kyr characteristic of the Vema Channel, according to Ledbetter (1979).

It is very clear, therefore, that sedimentation rates for calcareous contourites in the Ioffe Drift – Rio Grande Rise area are much lower than for mixed terrigenous-bioclastic contourites of the Santa Catarina – São Paulo Plateau and lower than most terrigenous contourites globally. We infer three principal reasons: (1) the Ioffe Drift– Rio Grande area is presently located within oligotrophic zone with extremely low surface biological productivity; (2) the region is far distant from any significant supply of terrigenous material; and (3) the vigorous activity of bottom currents has caused multiple erosional and non-depositional hiatuses.

As it was shown in Fig. 1a, the major branch of the LCDW/AABW outflow from the Vema Channel follows to the NE along the Florianopolis Fracture Zone being conveyed along the narrow deep channel at the base of the Ioffe Drift northern slope. According to modeling results (Frey et al., 2017, 2018), this flow deflects to the right creating an anticyclonic gyre above the drift summit. The gyre seems to possess more energy (Frey et al., 2018) than the return flow and gyre in the west, its erosional activity is likely also stronger, resulting in more common hiatuses on the Ioffe Drift.

According to Turnau and Ledbetter (1989), by 2.6–2.5 Ma a significant volume of southern-origin bottom water was introduced into the Rio Grande area. This timespan corresponds to the base of major erosional interval with numerous hiatuses in the Ioffe Drift cores, from 2.51/2.59 to ~1.9 Ma (Fig. 15; Ivanova et al., 2020, 2021). This might be explained by a stronger or shallower LCDW/AABW flow at that time, as proposed by Barker et al. (1983) for the Rio Grande area. In turn, the southward NADW flow in the Vema Channel, most probably with lower velocities than the underlying LCDW (Ledbetter, 1986), has influenced contourite deposition during MIS 8 to MIS 1 on the western flank of the Rio Grande Rise.

6.2. *A comparison with other CDSs*

By now, several CDSs are investigated from different parts of the globe (e.g. Hernández-Molina et al., 2008, 2009; Hernández-Molina et al., 2008, 2009 Faugères and Stow, 2008; Rebesco et al., 2014). Our new data provide a significant contribution to the current contourite knowledge, notably in terms of the deep-water biogenic calcareous CDSs, their specific and common features relative to the terrigenous deep-water CDSs, and mechanisms of formation. It is noteworthy that the Santa Catarina Plateau – São Paulo Plateau and the Ioffe Drift CDSs document yet poorly known influence of bottom waters of the Southern-origin on the sedimentation in the Atlantic.

The suggestion about variable bottom-current regime with periods of strong and weak bottom-current activity, demonstrated in our study, notably by the hiatuses, stiff horizons and erosion contacts associated with high hydrodynamics, is in line with the previous findings. The

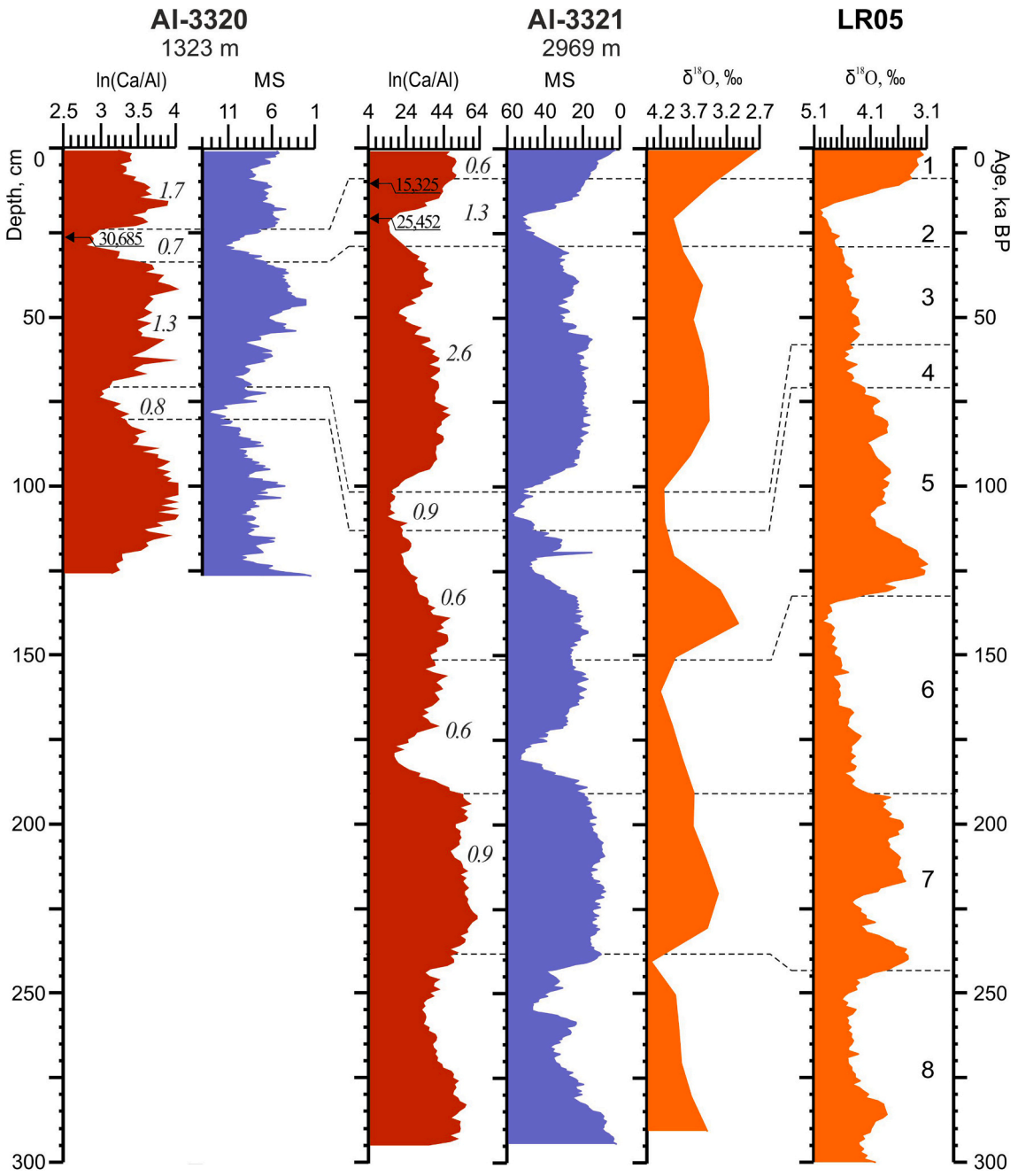

Fig. 16. Correlation of cores AI-3320 and AI-3321 from the Rio Grande Rise versus the oxygen isotope record LR05 (Lisiecki and Raymo, 2005). Cores AI-3320 and AI-3321 are correlated based on ln(Ca/Al) and volume magnetic susceptibility (MS, note reverted scale) records. Marine isotope stages and average sedimentation rates are indicated by numbers. The calibrated AMS ^{14}C dates from Table 3 are also shown.

inferences about the bottom current dynamics and footprints were made in several studies based on seismic and/or sedimentological data from different CDSs, including the Argentine and Uruguayan Continental Margin (Hernández-Molina et al., 2009; Wilckens et al., 2021), Rockall Plateau (Sayago-Gil et al., 2010), Demerara Plateau (Tallobre et al., 2016), Eirik Drift (Davies et al., 2021), Maurice Ewing Bank (Najjar-ifarizhendi and Uenzelmann-Neben, 2021), Mozambique Channel (Breitzke et al., 2017) and others.

According to Global contourite distribution database (Flanders Marine Institute et al., 2019), the contourite system on the Santa Catarina Plateau is a part of the Argentine slope CDS (http://marineregions.org/mrgid/30258) which also includes several giant drifts and sediment wave fields in the Argentine Basin, suitable for comparison. Sediment waves in the abyssal part of the Argentine Basin and those on the Santa Catarina Plateau show a number of similarities. They cover surfaces of large-scale drifts (Zapiola, Argiro, Ewind drift and Santa Catarina drift, respectively) (e.g., Ewing and Lonardi, 1971; Flood et al., 1993; Jeck et al., 2019). Areas of buried (not active) and non-buried (active) waves were found in both areas. The waves have comparable dimensions. They have typical heights of 25–30 m (up to 150 m) at wave lengths of 5–6 km (up to 10 km) in the Argentine Basin (Klaus and Ledbetter, 1988; Flood and Shor, 1988; Manley and Flood, 1993) and heights of 15–30 m (up to 60 m) at wave lengths of 2–4 km on the SCP (Borisov et al., 2020). The main difference is in the wave morphology and sedimentation rates. The wave field on the SCP is dominated by symmetric sediment waves without evidence of migration (Borisov et al., 2020). The average sedimentation rates in this area are generally lower than in the Argentine Basin, but close to one on the downslope wave flanks on the Zapiola

Drift (2–10 cm/kyr) (Jones, 1994). Sedimentation rates on the depositional wave flanks exceed 30 cm/kyr (Flood et al., 1993; Ledbetter, 1993). These differences can be explained by the strong variability of current speeds and directions on the SCP (Speer and Zenk, 1993; McDonagh et al., 2002; Frey et al., 2018) resulted in alternated deposition on different wave flanks (Borisov et al., 2020) and formation of short-term hiatuses.

The evidence of strong winnowing and reworking under high-energy conditions is provided by the siliciclastic sandy contourites, represented by well-sorted very fine to coarse sand occurring on the upper continental slope of the Mozambican margin, at about 300 m water depth (de Castro et al., 2021). The shallow-water bioclastic sandy and muddy contourites on the eastern flank of the Corsica Trough (at 370 m water depth) also suggest intermittent depositional conditions (de Castro et al., 2021). The strong winnowing by bottom currents here can be likely compared to the processes at the Rio Grande Rise summit demonstrated by the sediment composition and grain size data from our core AI-3320 (Figs. 11-13) since the Corsica sandy contourites also consist mostly of foraminiferal tests.

As many other carbonate drifts, the Ioffe Drift is located on the isolated buildup representing an obstacle for the currents (e.g. Mullins et al., 1980; Chabaud et al., 2016; Eberli and Betzler, 2019). One third of the known carbonate contourite depositional bodies (incl. Ioffe Drift) are elongated mounded drifts. The Ioffe Drift dimensions are comparable to drifts from the Little and Great Bahama Bank (e.g., Tournadour et al., 2015; Chabaud et al., 2016) and Marion Plateau (e.g., Eberli et al., 2010). The main distinguishing features of the drift are much greater water depth of the location, negligible sea-level influence on sediment source and composition and long-term hiatuses.

Unlike several other systems, notably from the North Atlantic (e.g. Hernández-Molina et al., 2008; Faugères and Stow, 2008; Rebesco et al., 2014), the CDSs from this study are characterized by rather low sedimentation rates. This is especially true for the calcareous sediments of the Ioffe Drift and partially for the Rio Grande Rise (Fig. 16) while the higher average rates are typical of the Santa Catarina Plateau – São Paulo Plateau contourites. On the one hand, this limits the paleoceanographic value of the studied CDSs, but, on the other hand, it enables a deeper penetration of our records into the geological time, notably on the Ioffe Drift.

7. Conclusions

Based on high-resolution seismic records, seafloor morphology and sediment/stratigraphic analyses from relatively short cores, a series of contourite drifts, sediment wave fields and erosional channel elements are identified in the South Atlantic Ocean near the northern exit of the Vema Channel. Two regions have been studied in detail: (1) the Santa Catarina Plateau – São Paulo Plateau area; and (2) the Ioffe Drift – Rio Grande Rise area.

The CDSs in the Ioffe Drift and Santa Catarina Plateau – São Paulo Plateau areas formed under the influence of a strong LCDW/AABW outflow from the Vema Channel, with variable bottom current speeds up to 30 cm/s according to Frey et al. (2018, 2022). A sediment wave field and mounded elongate contourite drift on the Santa Catarina Plateau along with a small contourite patch drifts on the southern escarpment of the São Paulo Plateau have developed under the influence of an anticyclonic gyre of LCDW, created from the westward branch of the outflow. In the Ioffe Drift area to the NE of the northern exit from the channel, another anticyclonic LCDW gyre controlled extensive erosion and reworking of contouritic sediments along with their lateral transport and accumulation. At a higher level in the water column, the southward flow of NADW through the Vema Channel favored contourite deposition on its eastern border, on the western flank of the Rio Grande Rise.

In the Santa Catarina Plateau – São Paulo Plateau area, the Middle Pleistocene to Holocene sediments show a range of characteristics typical of *terrigenous* contourites: (1) a lack of primary sedimentary structures, apart from some sharp erosional contacts, silty-sandy layers, stiff mud horizons, and indistinct bedding, (2) pervasive bioturbation, (3) mostly fine (silty) grain-size, very poor sorting, and distinctive bi-gradational sequences up to silty sand and sand size; (4) a high degree of correlation between the *SS* content of sortable silt in the total < 63 μm size fraction and *SS* mean sizes in all eight cores studied; and (5) a mixed terrigenous-biogenic composition, reflecting part hemipelagic input and part downslope sediment supply.

In the Ioffe Drift area, the *calcareous* contourite origin of the Upper Pliocene – Quaternary biogenic ooze is documented by the seismic structure of the upper sediment cover, pervasive bioturbation, bi-gradational sequences, poor to very poor sorting, missing and reduced thickness of biostratigraphic zones, and multiple hiatuses. It is also supported by rather high correlation coefficients between the apparent *SS* content of sortable silt in the total < 63 μm size fraction and *SS* mean sizes in four of six cores studied. Overall, these findings suggest vigorous LCDW/AABW outflow from the Vema Channel along the Florianopolis Fracture Zone and/or periodic events of high and variable bottom-current velocities leading to erosional events and hiatuses.

Although the mostly terrigenous (mixed composition) and calcareous (biogenic) contourites documented from the study areas differ in the sediment composition, both types are characterized by the occurrence of erosional contacts and hiatuses, layering (in some cases), pervasive bioturbation, mostly poor to very poor sorting, and more or less well-developed bi-gradational sequences. The terrigenous contourites are generally finer-grained and with a distinctive layering in parts. They demonstrate a marked glacial/interglacial stratigraphy, with greater biogenic accumulation during the sea-level highstands. The degree of correlation between content and mean size of *SS* in the fraction <63 μm as well as average sedimentation rates are higher in terrigenous contourites as compared to calcareous ones. Calcareous contourites contain ferromanganese nodules and more numerous erosional hiatuses. Calcareous contourites develop only above the lysocline.

Data availability

The data used in this paper are lodged with the Mendeley data repository:

- Ca/Al ratio in sediments from the Santa Catarina Plateau and the Ioffe Drift: https://doi.org/10.17632/ck58w4rstv.1
- Benthic oxygen isotopes from core AI-3321, Rio Grande Rise: https://doi.org/10.17632/pscjjb2gtz.1
- High-resolution seismoacoustic (sub-bottom) records from the Santa Catarina Plateau and the Ioffe Drift: https://doi.org/10.17632/zmpyrmvr66.1
- Volume magnetic susceptibility of sediments from the Ioffe Drift (South Atlantic): https://doi.org/10.17632/r59prx6dg6.1
- Mean particle size and sorting in sediments from the Santa Catarina Plateau and the Ioffe Drift: https://doi.org/10.17632/wygx9rtmwr.1

The detailed biostratigraphy of six Ioffe Drift's sediment cores is provided in Ivanova and Dmitrenko (2021), while the oxygen isotope data of the São Paulo' reference core AI-3152 (Ovsepyan and Ivanova, 2019) is available at https://doi.org/10.1016/j.palaeo.2018.10.031.

Declaration of Competing Interest

The authors declare that they have no known competing financial interests or personal relationships that could have appeared to influence the work reported in this paper.

Acknowledgments

The authors are grateful to scientific parties, masters and crews of the

R/V *Akademik Ioffe* (cruises 32, 33, 35, 37, 43, 46, 50, 52, 53) for their professional support in the material collection for this study. The grain-size analyses from the new cores were performed by E. Dorokhova, N. Nemchenko and E. Streltsova at the Shirshov Institute of Oceanology. The low-resolution oxygen isotope measurements from core AI-3321 were offered by D. Hodell (The Godwin Laboratory, Cambridge). We appreciate stimulating discussions with N. McCave. Special thanks to the Editors, Sara Rodrigues and two anonymous reviewers for their valuable comments and suggestions which helped us to improve the manuscript. The study was supported by the Russian Science Foundation grants 18-17-00227 and 22-27-00421.

References

Allen, M.B., Armstrong, H.A., 2008. Arabia–Eurasia collision and the forcing of mid-Cenozoic global cooling. Palaeogeogr. Palaeoclimatol. Palaeoecol. 265, 52–58.

Bacon, M.P., 1984. Glacial to interglacial changes in carbonate and clay sedimentation in the Atlantic Ocean estimated from ^{230}Th measurements. Chem. Geol. 46 (2), 97–111.

Barker, P.F., Carlson, R.L., Johnson, D.A., et al., 1983. Initial Reports of DSDP, Leg 72. U. S. Goverment Printing Office, Washington.

Bergen, J.A., Truax, S., de Kaenel, E., Blair, S., Browning, E., Lundquist, J., Boesiger, T., Bolivar, M., Clark, K., 2019. BP Gulf of Mexico Neogene astronomically-tuned time scale (BP GNATTS). Bull. Geol. Soc. Am. 131, 1871–1888. https://doi.org/10.1130/B35062.1.

Berggren, W.A., Aubry, M.P., Hamilton, N., 1983. Neogene magnetobiostratigraphy of Deep Sea drilling project site 516 (Rio Grande Rise, South Atlantic). In: Barker, P.F., Carlson, R.L., Johnson, D.A., et al. (Eds.), Initial Reports of DSDP, Leg 72. U.S. Government Printing Office, Washington, pp. 675–713.

Blott, S.J., Pye, K., 2001. Gradistat: a grain size distribution and statistics package for the analysis of unconsolidated sediments. Landforms 26, 1237–1248. https://doi.org/10.1002/esp.261.

Borisov, D., Levchenko, O., Libina, N., 2021. The Geomorphology and Seismic Structure. In: Murdmaa, I.O., Ivanova, E.V. (Eds.), The Ioffe Drift. Springer, Switzerland, pp. 37–51.

Borisov, D.G., Murdmaa, I.O., Ivanova, E.V., Levchenko, O.V., Yutsis, V.V., Frantseva, T. N., 2013. Contourite systems in the region of the southern São Paulo Plateau escarpment, South Atlantic. Oceanology 53, 460–471. https://doi.org/10.1134/S0001437013040012.

Borisov, D., Frey, D., Levchenko, O., 2020. Sediment waves on the Santa Catarina Plateau (western South Atlantic). J. S. Am. Earth Sci. 102, 102–698. https://doi.org/10.1016/j.jsames.2020.102698.

Bouma, A.H., 1964. Turbidites. Dev. Sedimentol. 3, 247–256. https://doi.org/10.1016/S0070-4571(08)70967-1.

Breitzke, M., Wiles, E., Krocker, R., Watkeys, M.K., Jokat, W., 2017. Seafloor morphology in the Mozambique Channel: evidence for long-term persistent bottom-current flow and deep- reaching eddy activity. Mar. Geophys. Res. 38, 241–269. https://doi.org/10.1007/s11001-017-9322-7 2017.

Chabaud, L., Ducassou, E., Tournadour, E., Mulder, T., Reijmer, J.J.G., Conesa, G., Giraudeau, J., Hanquiez, V., Borgomano, J., Ross, L., 2016. Sedimentary processes determining the modern carbonate periplatform drift of Little Bahama Bank. Mar. Geol. 378, 213–229. https://doi.org/10.1016/j.margeo.2015.11.006.

Chung, S.-N., Lee, K., Feely, R.A., Sabine, C.L., Millero, F.J., Wanninkhof, R., Bullister, J. L., Key, R.M., Peng, T.-H., 2003. Calcium carbonate budget in the Atlantic Ocean based on water column inorganic carbon chemistry. Glob. Biogeochem. Cycles 17 (4), 1093. https://doi.org/10.1029/2002GB002001.

Curry, W.B., Oppo, D.W., 2005. Glacial water mass geometry and the distribution of $\delta^{13}C$ of ΣCO_2 in the western Atlantic Ocean. Paleoceanography 20, PA1017. https://doi.org/10.1029/2004PA001021.

Damuth, J.E., Hayes, D.E., 1977. Echo character of the East Brazilian continental margin and its relationship to sedimentary processes. Mar. Geol. 24, 73–95. https://doi.org/10.1016/0025-3227(77)90002-0.

Davies, S., Stow, D., Nicholson, U., 2021. Late glacial to holocene sedimentary facies of the Eirik Drift, southern Greenland margin: Spatial and temporal variability and paleoceanographic implications. Mar. Geol. 440, 106568 https://doi.org/10.1016/j.margeo.2021.106568.

de Castro, S., Miramontes, E., Dorador, J., Jouet, G., Cattaneo, A., Rodríguez-Tovar, F.J., Hernández-Molina, F.J., 2021. Siliciclastic and bioclastic contouritic sands: Textural and geochemical characterisation. Mar. Pet. Geol. 128, 105002 https://doi.org/10.1016/j.marpetgeo.2021.105002.

Depetris, P.J., Griffin, J.J., 1968. Suspended load in the Río de la Plata Drainage Basin. Sedimentology 11, 53–60.

Dmitrenko, O.B., 1987. A detailed zonal scale of the quaternary bottom deposits based on coccoliths (on the Rio Grande rise in the Atlantic OIcean). Oceanology 27 (3), 460–464 (in Russian with English translation).

Du, J., Haley, B.A., Mix, A., 2020. Evolution of the global overturning circulation since the last Glacial Maximum based on marine authigenic neodymium isotopes. Quat. Sci. Rev. 241, 106396 https://doi.org/10.1016/j.quascirev.2020.106396.

Duarte, C.S.L., Viana, A.R., 2007. Santos drift system: Stratigraphic organization and implications for late Cenozoic palaeocirculation in the Santos Basin. In: Viana, A.R., Rebesco, M. (Eds.), Economic and Palaeoceanographic Significance of Contourite Deposits, Geological Society, London, Special Publication, vol. 276, pp. 171–198.

Eberli, G.P., Anselmetti, F.S., Isern, A.R., Deluis, H., 2010. Timing of changes in sea-level and currents along Miocene platforms on the Marion Plateau, Australia. Cenozoic Carbonate Systems of Australasia, SEPM Special Publication 95, 219–242.

Eberli, G.P., Betzler, C., 2019. Characteristics of modern carbonate contourite drifts. Sedimentology 66, 1163–1191. https://doi.org/10.1111/sed.12584.

Ewing, M., Lonardi, A.G., 1971. Sediment transport and distribution in the Argentine Basin. 5. Sedimentary structure of the Argentine margin, basin, and related provinces. Phys. Chem. Earth 8, 125–156. https://doi.org/10.1016/0079-1946(71)90017-6.

Faugères, J., Stow, D.A.V., 2008. Contourite Drifts: Nature, Evolution and Controls. Contourites. https://doi.org/10.1016/S0070-4571(08)10014-0.

Faugères, J.C., Stow, D.A.V., Imbert, P., Viana, A., 1999. Seismic features diagnostic of contourite drifts. Mar. Geol. 162 (1), 1–38.

Faugères, J.-C., Zaragosi, S., Mézerais, M.L., Massé, L., 2002. The Vema contourite fan in the south Brazilian basin. In: Stow, D.A.V., Pudsey, C.J., Howe, J.A., Faugères, J.-C., Viana, A.R. (Eds.), Deep-Water Contourite Systems: Modern Drifts and Ancient Series, Seismic and Sedimentary Characteristics. Geological Society, London, Memoir, vol. 22, pp. 209–222.

Flanders Marine Institute, Renard Centre of Marine Geology, University of Gent, 2019. Global Contourite Distribution Database, Version 3. https://doi.org/10.14284/346.

Flood, R.D., Shor, A.N., 1988. Mud waves in the Argentine Basin and their relationship to regional bottom circulation patterns. Deep Sea Res. Part A, Oceanogr. Res. Pap. 35, 943–971. https://doi.org/10.1016/0198-0149(88)90070-2.

Flood, R.D., Shor, A.N., Manley, P.L., 1993. Morphology of abyssal mudwaves at project MUDWAVES sites in the Argentine Basin. Deep. Res. Part II 40, 859–888. https://doi.org/10.1016/0967-0645(93)90038-O.

Folk, R.L., Ward, W.C., 1957. Brazos River bar: a study in the significance of grain size parameters. J. Sediment. Petrol. 27, 3–26.

Frey, D.I., Fomin, V.V., Diansky, N.A., Morozov, E.G., Neiman, V.G., 2017. New model and field data on estimates of Antarctic Bottom Water flow through the deep Vema Channel. Dokl. Earth Sci. 474, 561–564. https://doi.org/10.1134/S1028334X17050026.

Frey, D.I., Fomin, V.V., Tarakanov, R.Y., Diansky, N.A., Makarenko, N.I., 2018. Bottom water flows in the Vema Channel and over the Santos Plateau based on the field and numerical experiments. In: Velarde, M.G., Tarakanov, R.Y., Marchenko, A.V. (Eds.), The Ocean in Motion: Circulation, Waves, Polar Oceanography. Springer International Publishing, Cham, pp. 475–485. https://doi.org/10.1007/978-3-319-71934-4_29.

Frey, D., Borisov, D., Fomin, V., Morozov, E., Levchenko, O., 2022. Modeling of bottom currents for estimating their erosional-depositional potential in the Southwest Atlantic. J. Mar. Syst. 230, 103736 https://doi.org/10.1016/j.jmarsys.2022.103736.

Gauchery, T., Rovere, M., Pellegrini, C., Cattaneo, A., Campiani, E., Trincardi, F., 2021a. Factors controlling margin instability during the Plio-Quaternary in the Gela Basin (Strait of Sicily, Mediterranean Sea). Mar. Pet. Geol. 123, 104767.

Gauchery, T., Rovere, M., Pellegrini, C., Asioli, A., Tesi, T., Cattaneo, A., Trincardi, F., 2021b. Post-LGM multi-proxy sedimentary record of bottom-current variability and downslope sedimentary processes in a contourite drift of the Gela Basin (Strait of Sicily). Mar. Geol. 439, 106564 https://doi.org/10.1016/j.margeo.2021.106564.

Gingele, F.X., Schmieder, F., von Dobeneck, T., Petschick, R., Rühlemann, C., 1999. Terrigenous flux in the Rio Grande rise area during the past 1500 ka: evidence of Deepwater advection or rapid response to continental rainfall patterns? Paleoceanography 14 (1), 84–95.

Gonthier, E.G., Faugères, J.-C., Stow, D.A.V., 1984. Contourite facies of the Faro Drift, Gulf of Cadiz. Geol. Soc. Lond., Spec. Publ. 15 (1), 275. https://doi.org/10.1144/GSL.SP.1984.015.01.18.

Hanebuth, T.J., Zhang, W., Hofmann, A.L., Löwemark, L.A., Schwenk, T., 2015. Oceanic density fronts steering bottom-current induced sedimentation deduced from a 50 ka contourite-drift record and numerical modeling (off NW Spain). Quat. Sci. Rev. 112, 207–225.

Heaton, T.J., Köhler, P., Butzin, M., Bard, E., Reimer, R.W., Austin, W.E.N., Ramsey, C.B., Grootes, P.M., Hughen, K.A., Kromer, B., Reimer, P.J., Adkins, J., Burke, A., Cook, M. S., Olsen, J., Skinner, L., 2020. Marine20 - the marine radiocarbon age calibration curve (0–55,000 cal BP). Radiocarbon 62 (4), 779–820. https://doi.org/10.1017/RDC.2020.68.

Heezen, B.C., Hollister, C.D., Ruddiman, W.F., 1966. Shaping of the continental rise by deep geostrophic contour currents. Science 152, 502–508. https://doi.org/10.1126/science.152.3721.502.

Hernández-Molina, F.J., Llave, E., Somoza, L., Fernández-Puga, M.C., Maestro, A., Léon, R., Medialdea, T., Barnolas, A., García, M., del Río, V.D., Fernández-Salas, L. M., Vázquez, J.T., Lobo, F., Dias, J.M.A., Rodero, J., Gardner, J., 2003. Looking for clues to paleoceanographic imprints: a diagnosis of the Gulf of Cadiz contourite depositional systems. Geology 31 (1), 19–22. https://doi.org/10.1130/0091-7613(2003)031<0019:LFCTPI>2.0.CO;2.

Hernández-Molina, F.J., Llave, E., Stow, D.A.V., 2008. Continental slope contourites. In: Rebesco, M., Camerlenghi, A. (Eds.), Contourites, Developments in Sedimentology, vol. 60. Elsevier, Amsterdam, pp. 379–408. https://doi.org/10.1016/S0070-4571(08)10019-X.

Hernández-Molina, F.J., Paterlini, M., Somoza, L., Violante, R., Arecco, M.A., de Isasi, M., Rebesco, M., Uenzelmann-Neben, G., Neben, S., Marshall, P., 2010. Giant mounded drifts in the argentine Continental margin: Origins, and global implications for the history of thermohaline circulation. Mar. Pet. Geol. 27, 1508–1530. https://doi.org/10.1016/j.marpetgeo.2010.04.003.

Hernández-Molina, F.J., Paterlini, M., Violante, R., Marshall, P., de Isasi, M., Somoza, L., Rebesco, M., 2009. Contourite depositional system on the argentine slope: an exceptional record of the influence of Antarctic water masses. Geology 37, 507–510.

Hernández-Molina, F.J., Soto, M., Piola, A.R., Tomasini, J., Preu, B., Thompson, P., Badalini, G., Creaser, A., Violante, R.A., Morales, E., Paterlini, M., De Santa Anab, H., 2016. A contourite depositional system along the Uruguayan continental margin: sedimentary, oceanographic and paleoceanographic implications. Mar. Geol. 378, 333–349. https://doi.org/10.1016/j.margeo.2015.10.008.

Hodell, D.A., Charles, C.D., Sierro, F.J., 2001. Late Pleistocene evolution of the ocean's carbonate system. Earth Planet. Sci. Lett. 192, 109–124. https://doi.org/10.1016/S0012-821X(01)00430-7.

Hollister, C.D., McCave, I.N., 1984. Sedimentation under deep-sea storms. Nature 309, 220–225. https://doi.org/10.1038/309220a0.

Ivanova, E.V., 2009. The Global Thermohaline Paleocirculation. Springer, Dordrecht, Heidelberg.

Ivanova, E., Dmitrenko, O., 2021. Chapter 7. Micropaleontology and biostratigraphy. In: Murdmaa, I., Ivanova, E. (Eds.), The Ioffe Drift. Springer. https://doi.org/10.1007/978-3-030-82871-4_7.

Ivanova, E.V., Murdmaa, I.O., Borisov, D.G., Dmitrenko, O.B., Levchenko, O.V., Emelyanov, E.M., 2016a. Late Pliocene–Pleistocene stratigraphy and history of formation of the Ioffe calcareous contourite drift, Western South Atlantic. Mar. Geol. 372, 17–30. https://doi.org/10.1016/j.margeo.2015.12.002.

Ivanova, E.V., Murdmaa, I.V., Borisov, D.G., Isachenko, S.M., Seitkalieva, E.A., Bashirova, L.D., Blinova, E.V., Ulyanova, M.A., Lapidus, L.V., Fidaev, D.T., 2016b. Investigation of contourite systems in the South Atlantic during Cruise 46 of the R/V Akademik Ioffe. Oceanology 56, 322–324. https://doi.org/10.1134/S0001437016040044.

Ivanova, E.V., Murdmaa, I.O., Borisov, D.G., Ovsepyan, E.A., Simagin, N.V., Mutovkin, A. D., Nemchenko, N.V., Kornilova, M.O., Sud'in, V.V., Novikov Yu, V., 2018a. Study of lateral sedimentation in the Western Atlantic on Cruise 53 of the R/V Akademik Ioffe. Oceanology 58 (6), 932–934 (in Russian with English translation). https://doi.org/10.1134/S0001437018060073.

Ivanova, E.V., Murdmaa, I.O., Borisov, D.G., Simagin, N.V., Ovsepyan, E.A., Libina, N.V., Isola, J.I., Bulycheva, E.V., Shulga, N.A., Krek, A.V., Lobus, N.V., Lapidus, L.V., 2018b. Geological and geophysical investigation of contourite systems from the central and Southern Atlantic during cruise 52 of the R/V Akademik Ioffe. Oceanology 58 (5), 322–324 (in Russian with English translation). https://doi.org/10.1134/S0001437018020054.

Ivanova, E.V., Borisov, D.G., Dmitrenko, O.B., Murdmaa, I.O., 2020. Hiatuses in the late Pliocene-Pleistocene stratigraphy of the Ioffe calcareous contourite drift, western South Atlantic. Mar. Pet. Geol. 111, 624–637. https://doi.org/10.1016/j.marpetgeo.2019.08.031.

Ivanova, E., Borisov, D., Murdmaa, I., 2021. Chapter 9. Hiatuses and core correlations. In: Murdmaa, I., Ivanova, E. (Eds.), The Ioffe Drift. Springer. https://doi.org/10.1007/978-3-030-82871-4_9.

Jaccard, S.L., Haug, G.H., Sigman, D.M., Pedersen, T.F., Thierstein, H.R., Röhl, U., 2005. Glacial/interglacial changes in Subarctic North Pacific stratification. Science 308, 1003–1006. https://doi.org/10.1126/science.1108696.

Jackett, D.R., McDougall, T.J., 1997. A neutral density variable for the world's oceans. J. Phys. Oceanogr. 27, 237–263. https://doi.org/10.1175/1520-0485(1997)0272.0.CO;2.

Jeck, I.K., Alberoni, A.A.L., Torres, L.C., Zalán, P.V., 2019. The Santa Catarina Plateau and the nature of its basement. Geo-Marine Lett. https://doi.org/10.1007/s00367-019-00585-z.

Johnson, D.A., 1984. The Vema Channel: Physiography, structure, and sediment—current interactions. Mar. Geol. 58, 1–34. https://doi.org/10.1016/0025-3227(84)90114-2.

Johnson, D.A., Tappa, E., Thunell, R., 1984. Late tertiary/Quaternary magnetostratigraphy and biostratigraphy of Vema Channel sediments. Mar. Geol. 58 (1/2), 89–100.

Jones, G.A., 1994. Holocene climate and deep ocean circulation changes: Evidence from accelerator mass spectrometer radiocarbon dated Argentine Basin (SW Atlantic) mudwaves. Paleoceanography 9, 1001–1016. https://doi.org/10.1029/94PA01441.

Jones, G.A., Johnson, D.A., Curry, W.B., 1984. High-resolution stratigraphy in late Pleistocene/Holocene sediments of the Vema Channel. Mar. Geol. 58 (1/2), 59–87.

Jullion, L., Heywood, K.J., Naveira Garabato, A.C., Stevens, D.P., 2010. Circulation and water mass modification in the Brazil–Malvinas confluence. J. Phys. Oceanogr. 40, 845–864. https://doi.org/10.1175/2009JPO4174.1.

Kennett, J.P., Barker, P.F., 1990. Latest cretaceous to Cenozoic climate and oceanographic developments in the Weddell Sea, Antarctica: an ocean drilling perspective. In: Proceedings of the Ocean Drilling Program, Scientific Results, 113, pp. 937–960.

Klaus, A., Ledbetter, M.T., 1988. Deep-sea sedimentary processes in the Argentine Basin revealed by high-resolution seismic records (3.5 kHz echograms). Deep Sea Res. Part A, Oceanogr. Res. Pap. 35, 899–917. https://doi.org/10.1016/0198-0149(88)90067-2.

Krastel, S., Wefer, G., Hanebuth, T.J.J., Antobreh, A.A., Freudenthal, T., Preu, B., Schwenk, T., Strasser, M., Violante, R., Winkelmann, D., 2011. Sediment dynamics and geohazards off Uruguay and the de la Plata River region (northern Argentina and Uruguay). Geo-Mar. Lett. 31, 271–283. https://doi.org/10.1007/s00367-011-0232-4.

Laberg, J.S., Camerlenghi, A., 2008. The significance of Contourites for Submarine Slope Stability, First ed. Contourites. Elsevier. https://doi.org/10.1016/S0070- 4571(08)10025-5.

Le Pichon, X., Ewing, M., Truchan, M., 1971. Sediment transport and distribution in the Argentine Basin, 2. Antarctic bottom current passage into the Brazil Basin. In: Ahrens, L.H. (Ed.), Physics and Chemistry of the Earth, VIII, pp. 31–48.

Ledbetter, M.T., 1979. Fluctuations of Antarctic Bottom Water velocity in the Vema Channel during the last 160,000 years. Mar. Geol. 33, 71–89.

Ledbetter, M.T., 1984. Bottom-current speed in the Vema Channel recorded by particle-size of sediment fine-fraction. Mar. Geol. 58, 137–149.

Ledbetter, M.T., 1986. A Late Pleistocene time-series of bottom-current speed in the Vema Channel. Palaeogeogr. Palaeoclimatol. Palaeoecol. 53 (1), 97–105.

Levchenko, O.V., Murdmaa, I.O., 2013a. Strategy of the lithological and seismoacoustic research of the deep-water deposits along transatlantic geotraverses during cruise 32 of the R/V Akademik Ioffe in the autumn of 2010 (Kaliningrad to Ushuaia). Oceanology 53, 124–128. https://doi.org/10.1134/S0001437013010098.

Levchenko, O.V., Murdmaa, I.O., 2013b. Multidisciplinary investigations along the ransatlantic transect Ushuaia (argentine)-La manche strait: cruise 33 of the R/V Akademik Ioffe. Oceanology 53, 252–257. https://doi.org/10.1134/S0001437013010104.

Levchenko, O.V., Murdmaa, I.O., Ivanova, E.V., Mutovkin, A.D., Blinova, E.V., Borisov, D.G., Dremuchev, S.A., Isachenko, S.M., Konstantinova, N.P., Lapidus, L.V., Firstova, A.V., Frantseva, T.N., Yutsis, V.V., 2014. New result of the seismic facies analysis of the quaternary deposits in the western Atlantic. Dokl. Earth Sci. 458, 1256–1260. https://doi.org/10.1134/S1028334X14100080.

Ledbetter, M.T., 1993. Late pleistocene to holocene fluctuations in bottom-current speed in the Argentine Basin mudwave field. Deep Sea Res. Part II Top. Stud. Oceanogr. 40, 911–920. https://doi.org/10.1016/0967-0645(93)90040-T.

Levchenko, O.V., Borisov, D.G., Libina, N.V., 2020. Contourites and Gravitites on the Rio Grande rise, Southwest Atlantic Ocean (Seismoacoustic Data). Lithol. Miner. Resour. 55, 165–176. https://doi.org/10.31857/S0024497X20030039.

Levitus, S., Locarnini, R.A., Boyer, T.P., Mishonov, A.V., Antonov, J.I., Garcia, H.E., Baranova, O.K., Zweng, M.M., Johnson, D.R., Seidov, D., 2010. World Ocean atlas 2009. NOAA Atlas NESDIS, 68.

Lisiecki, L.E., Raymo, M.E., 2005. A Pliocene–Pleistocene stack of 57 globally distributedbenthic δ18O records. Paleoceanography 20, PA1003. https://doi.org/10.1029/2004PA001071.

Lisniowski, M.A., Harlamov, V., Frazao, E.P., Pessanha, I.B.M., Neto, A.A., 2017. Sediment waves on the Rio Grande Rise. In: 2017 IEEE/OES Acoustics in Underwater Geosciences Symposium (RIO Acoustics). IEEE, pp. 1–5. https://doi.org/10.1109/RIOAcoustics.2017.8349731.

Livermore, R.A., Nankivell, A.P., Eagles, G., Morris, P., 2005. Paleogene opening of Drake Passage. Earth Planet. Sci. Lett. 236, 459–470.

Livermore, R., Hillenbrand, C.D., Meredith, M., Eagles, G., 2007. Drake passage and cenozoic climate: an open and shut case? Geochem. Geophys. Geosyst. 8 https://doi.org/10.1029/2005GC001224 art. no. Q01005.

Llave, E., Hernández-Molina, F.J., García, M., Ercilla, G., Roque, C., Juan, C., Mena, A., Preu, B., Van Rooij, D., Rebesco, M., Brackenridge, R., Jané, G., Gómez-Ballesteros, M., Stow, D., 2019. Contourites along the Iberian Continental Margins: Conceptual and Economic Implications. Geol. Soc. Lond., Spec. Publ. https://doi.org/10.1144/sp476-2017-46.

Loncke, L., Droz, L., Gaullier, V., Basile, C., Patriat, M., Roest, W., 2009. Slope instabilities from echo-character mapping along the French Guiana transform margin and Demerara abyssal plain. Mar. Pet. Geol. 26, 711–723. https://doi.org/10.1016/j.marpetgeo.2008.02.010.

Lovell, J.P.B., Stow, D.A.V., 1981. Identification of ancient sandy contourites. Geology 9, 347. https://doi.org/10.1130/0091-7613(1981)9<347:IOASC>2.0.CO;2.

Maestro, A., Gallastegui, A., Moreta, M., Llave, E., Bohoyo, F., Druet, M., Navas, J., Mink, S., Fernández-Sáez, F., Catalán, M., Gómez-Ballesteros, M., Munoz-Martín, A., Granja-Bruna, J.L., 2021. Echo-character distribution in the Cantabrian margin and the Biscay abyssal plain. J. Maps 17, 533–542. https://doi.org/10.1080/17445647.2021.1973917.

Maldonado, A., Barnolas, A., Bohoyo, F., Escutia, C., Galindo-Zaldívar, J., Hernández-Molina, J., Jabaloy, A., Lobo, F.J., Nelson, C.H., Rodríguez-Fernández, J., Somoza, L., Vázquez, J.-T., 2005. Miocene to recent contourite drifts development in the northern Weddell Sea 667 (Antarctica). Glob. Planet. Chang. 45, 99–129.

Manley, P.L., Flood, R.D., 1993. Paleoflow history determined from mudwave migration: Argentine Basin. Deep. Res. Part II Top. Stud. Oceanogr. 40, 1033–1055. https://doi.org/10.1016/0967-0645(93)90047-Q.

McCave, I.N., Manighetti, B., Robinson, S.G., 1995. Sortable silt and fine sediment size/composition slicing: parameters for paleocurrent speed and paleoceanography. Paleoceanography 1 (10), 593–610. https://doi.org/10.1029/94PA03039.

McCave, I.N., Thornelly, D.J.R., Hall, I.R., 2017. Relation of sortable silt grain-size to deep-sea current speeds: Calibration of the 'Mud Current Meter'. Deep-Sea Res. Part I. 127, 1–12. https://doi.org/10.1016/j.dsr.2017.07.003.

McDonagh, E.L., Arhan, M., Heywood, K.J., 2002. On the circulation of bottom water in the region of the Vema Channel. Deep-Sea Res. Part I Oceanogr. Res. Pap. 49, 1119–1139. https://doi.org/10.1016/S0967-0637(02)00016-X.

Meisling, K.E., Cobbold, P.R., Mount, V.S., 2001. Segmentation of an obliquely rifted margin, Campos and Santos basins, southeastern Brazil. AAPG Bull. 85 (11), 1903–1924.

Melguen, M., Thiede, J., 1974. Facies distribution and dissolution depths of surface sediment components from the Vema Channel and the Rio Grande rise (Southwest Atlantic Ocean). Mar. Geol. 17, 341–353.

Merrifield, M.A., Holloway, P.E., Johnston, T.M.S., 2001. The generation of internal tides at 678 the Hawaiian Ridge. Geophys. Res. Lett. 28, 559–562.

Mézerais, M.-L., Faugéeres, J.-C., Figueiredo, A.G., Massé, L., 1993. Contour current accumulation off the Vema Channel mouth, southern Brazil Basin: pattern of a "contourite fan". Sediment. Geol. 82, 173–187. https://doi.org/10.1016/0037-0738(93)90120-T.

Miramontes, E., Cattaneo, A., Jouet, G., Théreau, E., Thomas, Y., Rovere, M., Cauquil, E., Trincardi, F., 2016. The Pianosa Contourite Depositional System (Northern Tyrrhenian Sea): Drift morphology and Plio-Quaternary stratigraphic evolution. Mar. Geol. 378, 20–42. https://doi.org/10.1016/j.margeo.2015.11.004.

Mitchum, R.M.J., Vail, P.R., Sangree, J.B., 1977. Stratigraphic interpretation of seismic reflection patterns in depositional sequences. In: Payton, C.E. (Ed.), Seismic Stratigraphy: Applications to Hydrocarbon Exploration, vol. 26. the American Association of Petroleum Geologist, Tulsa, pp. 117–133.
Morozov, E.G., Demidov, A.N., Tarakanov, R.Y., Zenk, W., 2010. Abyssal Channels in the Atlantic Ocean. Springer, Dordrecht.
Morozov, E.G., Frey, D.I., Neiman, V.G., Makarenko, N.I., Tarakanov, R.Y., 2019. Extreme transport velocities of Antarctic Bottom Water flow through the deep Vema channel. Доклады АкадеМии наук 486, 485–488. https://doi.org/10.31857/S0869-56524864485-488.
Morozov, E.G., Frey, D.I., Tarakanov, R.Y., 2020. Flow of Antarctic bottom water from the Vema channel. Geosci. Lett. 7, 16. https://doi.org/10.1186/s40562-020-00166-4.
Murdmaa, I., Ivanova, E. (Eds.), 2021. The Ioffe Drift. Springer.
Mullins, H.T., Neumann, A.C., Wilber, R.J., Hine, A.C., Chinburg, S.J., 1980. Carbonate sediment In northern straits of Florida. AAPG Bull. American Assoc. Pet. Geol. 64, 1707–1717.
Murdmaa, I., Borisov, D., Dorokhova, E., Dara, O., 2021a. Chapter 6. Lithology. In: Murdmaa, I., Ivanova, E. (Eds.), The Ioffe Drift. Springer. https://doi.org/10.1007/978-3-030-82871-4_6.
Murdmaa, I., Ivanova, E., Borisov, D., 2021b. Chapter 10. History of the Ioffe Drift. In: Murdmaa, I., Ivanova, E. (Eds.), The Ioffe Drift. Springer. https://doi.org/10.1007/978-3-030-82871-4_10.
Najjarifarizhendi, B., Uenzelmann-Neben, G., 2021. Footprints of palaeocurrents in sedimentary sequences of the Cenozoic across the Maurice Ewing Bank. Mar. Geol. 438, 106525 https://doi.org/10.1016/j.margeo.2021.106525.
Orsi, A.H., Johnson, G.C., Bullister, J.L., 1999. Circulation, mixing, and production of antarctic bottom water. Prog. Oceanogr. 43, 55–109. https://doi.org/10.1016/S0079-6611(99)00004-X.
Ovsepyan, E.A., Ivanova, E.V., 2019. Glacial–interglacial interplay of southern- and northern-origin deep waters in the São Paulo Plateau – Vema Channel area of the western South Atlantic. Palaeogeogr. Palaeoclimatol. Palaeoecol. 514, 349–360. https://doi.org/10.1016/j.palaeo.2018.10.031.
Palomino, D., Vázquez, J.-T., Ercilla, G., Alonso, B., López-González, N., Díaz-del-Río, V., 2011. Interaction between seabed morphology and water masses around the seamounts on the Motril marginal Plateau (Alboran Sea, Western Mediterranean). Geo-Mar. Lett. 31, 465–479. https://doi.org/10.1007/s00367-011-0246-y.
Pellegrini, C., Maselli, V., Trincardi, F., 2016. Pliocene–Quaternary contourite depositional system along the south-western Adriatic margin: changes in sedimentary stacking pattern and associated bottom currents. Geo-Marine Lett. 36, 67–79.
Perez, L., García-Rodriguez, F., Hanebuth, T.J.J., 2016. Variability in terrigenous sediment supply offshore of the Río de la Plata (Uruguay) recording the continental climatic history over the past 1200 years. Clim. Past 12, 623–634. https://doi.org/10.5194/cp-12-623-2016.
Preu, B., Hernández-Molina, F.J., Violante, R., Piola, A.R., Paterlini, C.M., Schwenk, T., Voigt, I., Krastel, S., Spiess, V., 2013. Morphosedimentary and hydrographic features of the northern argentine margin: the interplay between erosive, depositional and gravitational processes and its conceptual implications. Deep. Res. Part I Oceanogr. Res. Pap. 75, 157–174. https://doi.org/10.1016/j.dsr.2012.12.013.
Razik, S., Chiessi, C.M., Romero, O.E., Dobeneck, T., 2013. Interaction of the South American Monsoon system and the southern westerly wind belt during the last 14 kyr. Palaeogeogr. Palaeoclimatol. Palaeoecol. 374, 28–40. https://doi.org/10.1016/j.palaeo.2012.12.022.
Rebesco, M., 2005. Contourites. In: Selley, R.C., Cocks, L.R.M., Plimer, I.R. (Eds.), Encyclopedia of Geology. Elsevier, Oxford, pp. 513–527.
Rebesco, M., Camerlenghi, A., 2008. Contourites (Elseiver).
Rebesco, M., Hernández-Molina, F.J., Van Rooij, D., Wahlin, A., 2014. Contourites and associated sediments controlled by deep-water circulation processes: State-of-the-art and future considerations. Mar. Geol. 352, 111–154.
Rebesco, M., Stow, D., 2001. Seismic expression of contourites and related deposits: a preface. Mar. Geophys. Res. 22, 303–308. https://doi.org/10.1023/A:1016316913639.
Rickaby, R.E.M., Elderfield, H., Roberts, N., Hillenbrand, C.-D., Mackensen, A., 2010. Evidence for elevated alkalinity in the glacial Southern Ocean. Paleoceanography 25 (1), PA1209. https://doi.org/10.1029/2009PA001762.
Robinson, S.G., McCave, I.N., 1994. Orbital forcing of bottom-current enhanced sedimentation on Feni Drift, NE Atlantic, during the mid-Pleistocene. Paleoceanography 9 (6), 943–972. https://doi.org/10.1029/94PA01439.
Rothwell, R.G., Croudace, I.W., 2015. Twenty years of XRF core scanning marine sediments: what do geochemical proxies tell us? In: Croudace, I., Rothwell, R. (Eds.), Micro-XRF Studies of Sediment Cores, Developments in Paleoenvironmental Research, vol. 17. Springer, Dordrecht, pp. 25–102. https://doi.org/10.1007/978-94-017-9849-5_2.
Rovere, M., Pellegrini, C., Chiggiato, J., Campiani, E., Trincardi, F., 2019. Impact of dense bottom water on a continental shelf: an example from the SW Adriatic margin. Mar. Geol. 408, 123–143.
Sayago-Gil, M., Long, D., Hitchen, K., Díaz-del-Río, V., Fernández-Salas, L.M., Durán-Muñoz, P., 2010. Evidence for current-controlled morphology along the western slope of Hatton Bank (Rockall Plateau, NE Atlantic Ocean). Geo-Mar. Lett. 30, 99–111. https://doi.org/10.1007/s00367-009-0163-5.
Schlitzer, R., 2010. Ocean data view. In: Ocean Data View 4.7.10. http://odv.awi.de.
Schlumberger, 2022. Oilfield Glossary. https://glossary.oilfield.slb.com/en/terms/r/reflector (accessed 13 April 2022).
Schmieder, F., 2004. Magnetic signals in Plio-Pleistocene sediments of the South Atlantic:Chronostratigraphic usability and paleoceanographic implications. In: Wefer, G., Mulitza, S., Ratmeyer, V. (Eds.), The South Atlantic in the Late Quaternary:Reconstruction of Material Budgets and Current Systems. Springer-Verlag, pp. 263–279.
Shepard, F.P., 1954. Nomenclature based on sand-silt-clay ratios. J. Sediment. Petrol. 24 (3), 151–158.
Shulga, N., Murdmaa, I., Dara, O., Ryazanztsev, K., 2021. Chapter 8. Ferromanganese nodules. In: Murdmaa, I., Ivanova, E. (Eds.), The Ioffe Drift. Springer. https://doi.org/10.1007/978-3-030-82871-4_8.
Skolotnev, S.G., Ivanova, E.V., Murdmaa, I.O., Peyve, A.A., Borisov, D.G., Isachenko, S.M., Blinova, E.V., Zinger, T.F., Kravtsov, V.A., Ovsepyan, E.A., Seitkalieva, E.A., Ulyanova, M.O., Fidaev, D.T., 2018. Study of seamounts and contourite systems of the Central and South Atlantic during Cruise 43 of the R/V Akademik Ioffe. Oceanology 58 (4), 671–673. https://doi.org/10.1134/S0001437018040094.
Speer, K.G., Zenk, W., 1993. The flow of Antarctic Bottom Water into the Brazil Basin. J. Phys. Ocean. 23 (12), 2667–2682.
Stow, D.A.V., Faugères, J.-C., 2008. Chapter 13 Contourite facies and the facies model. In: Rebesco, M., Camerlenghi, A. (Eds.), Contourites, Developments in Sedimentology, vol. 60. Elsevier, Amsterdam, pp. 223–256. https://doi.org/10.1016/S0070-4571(08)10013-9.
Stow, D.A.V., Smillie, Z., 2020. Distinguishing between Deepwater sediment facies: turbidites, contourites and hemipelagites. Geosciences 10 (2), 68. https://doi.org/10.3390/geosciences10020068.
Stow, D.A.V., Kahler, G., Reeder, M., 2002. Fossil contourites: Type example from an Oligocene palaeoslope system, Cyprus. In: Stow, D.A.V., Pudsey, C.J., Howe, J.A., Faugères, J.-C., Viana, A.R. (Eds.), Deep-Water Contourite Systems: Modern Drifts and Ancient Series, Seismic and Sedimentary Characteristics, Geological Society, London, Memoir, vol. 22, pp. 443211–443455.
Stow, D.A.V., Hernández-Molina, F.J., Llave, E., Bruno, M., García, M., Díaz del Río, V., Somoza, L., Brackenridge, R.E., 2013. The Cadiz Contourite Channel: sandy contourites, bedforms and dynamic current interaction. Mar. Geol. 343, 99–114. https://doi.org/10.1016/j.margeo.2013.06.013.
Stow, D.A.V., Smillie, Z., Pan, J., Esentia, I., 2019. Deep-Sea contourites: sediments and cycles. In: Encyclopedia of Ocean Sciences. Elsevier, pp. 111–120. https://doi.org/10.1016/B978-0-12-409548-9.10879-6.
Stuiver, M., Reimer, P.J., Reimer, R.W., 2021. CALIB 8.2 [WWW Program]. http://calib.org (accessed 2021-2-18).
Tallobre, C., Loncke, L., Bassetti, M.A., Giresse, P., Bayon, G., Buscail, R., de Madron, X.D., Bourrin, F., Vanhaesebroucke, M., Sotin, C., 2016. Description of a contourite depositional system on the Demerara Plateau: Results from geophysical data and sediment cores. Mar. Geol. 378, 56–73. https://doi.org/10.1016/j.margeo.2016.01.003.
Thompson, R., Oldfield, F., 1986. Mineral magnetism in marine sediments. In: Environmental Magnetism. Springer, Netherlands, Dordrecht, pp. 141–152. https://doi.org/10.1007/978-94-011-8036-8_12.
Thran, A.C., Dutkiewicz, A., Spence, P., Müller, R.D., 2018. Controls on the global distribution of contourite drifts: Insights from an eddy-resolving ocean model. Earth Planet. Sci. Lett. 489, 228–240. https://doi.org/10.1016/j.epsl.2018.02.044.
Tournadour, E., Mulder, T., Borgomano, J., Hanquiez, V., Ducassou, E., Gillet, H., 2015. Origin and architecture of a mass transport complex on the northwest slope of Little Bahama Bank (Bahamas): relations between off-bank transport, bottom current sedimentation and submarine landslides. Sediment. Geol. 317, 9–26. https://doi.org/10.1016/j.sedgeo.2014.10.003.
Turnau, R., Ledbetter, M.T., 1989. Deep circulation changes in the South Atlantic Ocean: Response to initiation of northern hemisphere glaciation. Paleoceanography 4, 565–583. https://doi.org/10.1029/PA004i005p00565.
Viana, A., Figueiredo, A.G., Faugères, J.C., Lima, A., Gonthier, E., Brehme, I., Zaragosi, S., 2003. The São Tomé deep-sea turbidite system (Southern Brazil Basin): cenozoic seismic stratigraphy and sedimentary processes. AAPG (Am. Assoc. Pet. Geol.) Bull. 87, 873–894. https://doi.org/10.1306/12100201048.
Wade, B.S., Pearson, P.N., Berggren, W.A., Palike, H., 2011. Review and revision of Cenozoic tropical planktonic foraminiferal biostratigraphy and calibration to the geomagnetic polarity and astronomical time scale. Earth Sci. Rev. 104, 111–142.
Weltje, G.L., Tjallingii, R., 2008. Calibration of XRF core scanners for quantitative geochemical logging of sediment cores: Theory and application. Earth Planet. Sci. Lett. 274, 423–438.
Wilckens, H., Miramontes, E., Schwenk, T., Artana, C., Zhang, W., Piola, A.R., Baques, M., Provost, C., Hernández-Molina, F.J., Felgendreher, M., Spieß, V., Kasten, S., 2021. The erosive power of the Malvinas Current: Influence of bottom currents on morpho-sedimentary features along the northern Argentine margin (SW Atlantic Ocean). Mar. Geol. 439, 106539 https://doi.org/10.1016/j.margeo.2021.106539.
Wynn, R.B., Stow, D.A.V., 2002. Classification and characterisation of deep-water sediment waves. Mar. Geol. 192, 7–22. https://doi.org/10.1016/S0025-3227(02)00547-9.